Final Draft

Publication: Journal of Geotechnical and Geoenvironmental Engineering, Volume 148, Issue 7

https://ascelibrary.org/doi/10.1061/%28ASCE%29GT.1943-5606.0002813

This manuscript was submitted on February 10, 2021; approved on February 18, 2022; published online on May 11, 2022.

Published (print) in Volume 148, Issue 7: July 1, 2022

Kinematic soil-pile interaction under earthquake-induced non-linear soil and pile behaviour: An equivalent-linear approach

Stefano Stacul[1], Emmanouil Rovithis[2] and Raffaele Di Laora[3*]

[1] Department of Civil and Industrial Engineering, University of Pisa, 56122 Pisa, Italy

[2] Institute of Engineering Seismology and Earthquake Engineering (ITSAK), 55535 Thessaloniki, Greece

[3] Department of Engineering, University of Campania "Luigi Vanvitelli", 81031 Aversa (CE), Italy

[*]Corresponding Author, raffaele.dilaora@unicampania.it

Abstract

Kinematic bending and filtering potential of a fixed-head pile are explored when large shear strains are generated in the surrounding soil during the passage of seismic waves. The problem is treated numerically by employing a freely available 1D code to derive soil response at free-field conditions and an advanced 3D Finite-Difference (FD) model of the soil-pile system. Three idealized soil profiles with varying stiffness and strength and a real layered site are considered under earthquake excitation of increasing intensity, allowing investigation of the pile's non-linear kinematic response under shear strains exceeding the threshold of an equivalent-linear approximation. Simple analytical solutions are revisited in the context of soil response close to failure, by means of the FD solution, and an equivalent linear approach is proposed for assessing kinematic pile-head bending and filtering action in the presence of large earthquake-induced shear strains in the soil and non-linear pile behaviour. A practice-oriented procedure requiring only a pertinent 1D soil response analysis is reported to address kinematic effects in seismic design of piles.

INTRODUCTION

Besides inertial forces and moments coming from the oscillation of the superstructure, piles in earthquake-prone areas must be designed to withstand additional loading induced by the deformation of the surrounding soil during the passage of seismic waves. This particular type of loading originates from the kinematic interaction between pile and soil, which forces the pile to deform along its whole length, thus imposing additional bending on the pile. Under certain conditions, the kinematic-induced bending at the pile-head or at deeper elevations close to interfaces with sharp stiffness contrast may be more important than pile bending due to inertial forces. This has been established by post-earthquake observations in non-liquefiable soils (Tazoh et al. 1987; Mizuno, 1987; Nikolaou et al. 2001), which identified pile failures at depths where forces transmitted to the piles from the superstructure are negligible. The issue has received considerable attention by the geotechnical research community and a large number of simplified formulae are available to derive kinematic pile bending at the head of the pile (de Sanctis et al., 2010; Di Laora et al., 2013, Stacul and Squeglia 2020) or at an interface between successive soil layers (Dobry and O'Rourke, 1983; Mylonakis, 2001; Nikolaou et al., 2001; Maiorano et al., 2009; Dezi et al., 2010; Sica et al., 2011; Di Laora et al., 2012).

A concurrent phenomenon related to kinematic soil-pile interaction has been documented by field measurements on instrumented structures (Kawamura et al. 1977; Otha et al. 1980; Gazetas 1984). Upon comparing earthquake records between the foundation level of pile-supported buildings and the ground surface at free-field conditions, the above studies revealed the potential of piles to reduce the seismic motion which is actually transmitted to the superstructure [i.e. the Foundation Input Motion (FIM)] with respect to the free-field motion. Such a potential is referred to as the '*filtering effect'* of piles (Gazetas 1984; Mamoon and Banerjee 1990). The associated physical mechanism has been attributed to the inability of the pile, due to its stiffness, to follow short wavelengths of the free-field motion and thus filtering the high-frequency components of the surface motion (Florres-Berrones and Whitman 1982; Kaynia and Kausel 1991; Nikolaou et al. 2001; Anoyatis et al. 2013, Di Laora and de Sanctis 2013; Rovithis et al. 2013). A holistic interpretation of the filtering action of piles has been very recently suggested (Iovino et al. 2019; Di Laora and Rovithis 2021) by considering that piles average the non-uniform profile of displacement imposed by the surrounding soil along a fraction of the pile's active length. It is thus evident that the prediction of pile-head kinematic bending and FIM relies upon proper modelling of soil response at free-field conditions to estimate the ground surface motion and the deformation demand which the soil tries to impose on the pile.

When soil response is far from failure, the Equivalent Linear (EL) method allows a reliable prediction of soil response in free-field conditions up to some threshold shear strain that may be in the order of 0.2-0.4% (Kaklamanos et al. 2013), as it considers, in an approximate manner, soil stiffness degradation and hysteretic damping increase with increasing strain. In this case, simplified methods which are available in the literature for the assessment of the kinematic pile-head bending moments (Di Laora and Rovithis 2015) and the Foundation Input Motion (Iovino et al. 2019), referring to a continuously inhomogeneous soil with stiffness varying with depth according to a generalized power law, give reliable predictions, provided that the mobilized stiffness of the soil, associated to the earthquake-induced shear strains in free-field conditions, is employed in the formulae.

When larger strains are generated like in the case of soft soils under strong earthquake shaking, the assumption of a stiffness-controlled soil response, which is employed in the EL approximation, is no longer true, since the shear strength of the soil plays a dominant role and, therefore, soil response cannot be captured by considering its stiffness degradation alone (Shi and Assimaki 2017). In this case, while ground response may be assessed by means of freely-available software like DEEPSOIL (Hashash et al. 2016), provided that the stiffness and strength properties of the geotechnical configuration at hand are available from field and laboratory investigations, the only way to carry out a reliable design of piles seems to be the use of complex numerical analyses with advanced constitutive models for both the soil and the pile. Upon considering that such a task is not affordable in routine engineering, a question arises: Are the analytical formulae proposed in Di Laora and Rovithis 2015 and Iovino et al. 2019 for kinematic pile-head bending and foundation input motion, respectively, still applicable by properly adapting their input parameters in the presence of shear strains close to soil failure and non-linear pile behaviour?

This paper addresses the above nontrivial concerns via numerical analyses by employing experimentally validated soil constitutive models, referring to three idealized soil profiles with different stiffness and strength properties and a real layered site from the Po plain region of Northern Italy. A simple, practice-oriented procedure is proposed, which allows the prediction of pile kinematic response under strong non-linear soil and pile behaviour.

PROBLEM STATEMENT

The system under study consists of a single fixed-head pile embedded in a 30m thick soil layer resting on a rigid base (Fig.1). The pile is considered as a linearly elastic cylindrical solid beam of diameter d =1 m, length L = 20 m, Poisson's ratio ν_p = 0.15, unit weight ρ_p = 24 kN/m^3 and elastic modulus E_p =25 GPa. However, the non-linear behaviour of the pile's section may be equally considered in the framework of the proposed procedure through a pertinent moment-curvature relation, as it will be shown in the ensuing. The particular value of L should not be viewed as one established for design purposes involving the bearing capacity of the pile, in which case a larger value allowing pile tip penetration to the underlying rock would be required. Nevertheless, with reference to pile-head bending, L has practically no effect if it is larger than the “active” length (L_a) of the pile, which may be considered on the order of (8 - 10) d as a first approximation. Therefore, increasing the length of the pile beyond its active length will not affect kinematic bending at the head of the pile. Taking into account that the above condition (i.e. $L > L_a$) is satisfied almost for any pile, it can be asserted that the results of this study may be applied in all practical cases. Three soil profiles referring to a dry sand, an over-consolidated clay and a normally-consolidated clay are employed. The low-strain stiffness and strength properties of these soils are described in the ensuing.

Dry sand

The Hardin and Richart (1963) formula for round-grained sands was employed to obtain the distribution of the low-strain shear modulus (G_0) for the sandy soil as:

$$G_0(kPa) = 3300\frac{(2.97-e)^2}{1+e}\sqrt{\sigma'_{v0}} \tag{1}$$

where e is the void ratio and σ'_{v0} is the vertical effective geostatic stress. Upon assuming $e = 0.6$ and a unit weight (γ_s) of the soil particles equal to 26.5 kN/m^3, the dry unit weight (γ_d) of the sand is equal to 16.2 kN/m^3 while G_0 and the associated shear wave propagation velocity (V_{s0}) profiles can be cast in the simplified forms:

$$G_0(MPa) = 47z^{0.5} \tag{2}$$

and

$$V_{s0}(m/s) = 170z^{0.25} \tag{3}$$

where z [measured in m] is the depth from the ground surface. In this case, the average shear wave velocity in the first 30 m ($V_{s,30}$) is 300 m/s, which corresponds to soil type C according to EC8

(CEN 2004). The angle of internal friction (φ) is considered equal to 35.5° while the Poisson's ratio (ν) was set equal to 0.3.

Over-Consolidated (OC) Clay

The second profile under consideration is a fully-saturated, over-consolidated (OC) clay. The ratio ($\mathrm{s_u/\sigma'_{v0}}$) of the undrained shear strength (s_u) over the vertical effective geostatic stress for an OC clay can be derived by (Ladd et al. 1977):

$$\left(\frac{s_u}{\sigma'_{v0}}\right)_{OC} = \left(\frac{s_u}{\sigma'_{v0}}\right)_{NC} OCR^{0.8} \tag{4}$$

where OCR stands for the overconsolidation ratio and $\mathrm{(s_u/\sigma'_{v0})_{NC}}$ refers to a normally consolidated (NC) clay, which in turn can be estimated by the well-known formula of Skempton (1957):

$$\left(\frac{s_u}{\sigma'_{v0}}\right)_{NC} = 0.11 + 0.0037 I_p \tag{5}$$

In the above expression, I_P is the plasticity index. Upon considering I_P = 40% and OCR = 5, Equation 4 yields $\mathrm{(s_u/\sigma'_{v0})_{OC}}$ = 1.3. For the above parameters, a constant value of the shear strength s_u with depth may be considered as a realistic assumption, which can be derived by considering the effective geostatic stress at one half of the pile's length:

$$s_{u,OC}(kPa) = 1.3(\gamma_{sat} - \gamma_w)\frac{L}{2} \tag{6}$$

In this expression, γ_{sat} (= 17.9 kN/m^3) and γ_w correspond to the unit weight of the saturated soil and the unit weight of the water, respectively, yielding an undrained shear strength equal to 105 kPa. With reference to the low-strain shear modulus of the OC Clay profile, a proportionality relationship between G_0 and s_u was assumed as (Weiler 1988)

$$G_0 = 600 s_u \tag{7}$$

which yields G_0 = 35 MPa, denoting a homogeneous layer with constant shear modulus with depth, while Poisson's ratio (ν) was set at 0.495. In this case, $V_{s,30}$ is equal to 140 m/s, corresponding to soil type D according to EC8.

Normally-consolidated (NC) Clay

A fully saturated normally-consolidated (NC) clay is considered as a third soil type having the same values of γ_{sat} and I_P such as those employed for the OC clay. In this case, Equation 5 yields

$$s_{u,NC} = 0.258\sigma'_{v0} \tag{8}$$

or, equivalently,

$$s_{u,NC}(kPa) = 2.1z \tag{9}$$

Again, the low-strain shear modulus G_0 is considered proportional to depth by employing this time a larger multiplier of the associated shear strength profile, following Vardanega and Bolton (2013):

$$G_0 = 800s_u \tag{10}$$

In this manner, the distribution of G_0 with depth is given by:

$$G_0(MPa) = 1.7z \tag{11}$$

and the corresponding shear wave velocity profile may be described by:

$$V_{s0} = 30z^{0.5} \tag{12}$$

In this case, $V_{s,30}$ is equal to 100 m/s, corresponding again to soil type D according to EC8. The above expression was also adopted by Travasarou and Gazetas (2004) to model the stiffness variation with depth of a particularly soft, normally consolidated clay in a real site. The above low-strain stiffness and strength profiles for the three soils are plotted in Fig. 1.

Base excitations

The problem at hand is explored under seismic loading imposed at the base of the soil layer, in the form of vertically propagating SH waves. To this end, a set of seven earthquake recordings were selected from the PEER Strong Motion Database (Ancheta et al. 2013), upon setting the following criteria: (i) motions that have been recorded in rock-like formations, corresponding to soil type A according to EC8 and (ii) motions that cover a wide range of frequencies for earthquake engineering applications. The 5%-damped acceleration response spectra of the selected motions normalized by the peak rock acceleration (PRA) are plotted in Fig. 2. Relevant metadata of the earthquakes are listed in Table 1. Three levels of increasing intensity of the input motion were examined by scaling the selected records to three levels of Peak Rock Acceleration (PRA) considered at 0.10g, 0.15g and 0.25g, accordingly.

NUMERICAL ANALYSES: ELASTIC PILE RESPONSE

Two sets of numerical analyses were performed. The first set refers to one-dimensional free-field soil response analysis by means of the freely available code DEEPSOIL v.6.1, involving both equivalent linear (EL) and non-linear (NL) constitutive laws to model soil behaviour (Hashash et al. 2016). The Finite-Difference (FD) code FLAC3D v.6.0 (Itasca 2017) was then employed to perform a second series of non-linear time history analyses by implementing an advanced 3D model of the soil-pile system with pertinent laws of soil behaviour. Critical aspects of the numerical models including calibration procedures to obtain meaningful comparisons of the free-field response between the two codes are described in the following.

Constitutive laws in DEEPSOIL models

With reference to the Equivalent Linear (EL) analyses performed with DEEPSOIL, the degradation of the shear modulus (in the form of G/G_0 ratio) and the increase of the hysteretic damping (D) of the soil with increasing shear strain (γ) were modelled by implementing the $G/G_0 - \gamma - D(\%)$ curves proposed in Vucetic and Dobry (1991) for the OC and the NC clay at the assumed value of the plasticity index I_p = 40%. For the sandy soil, the upper limit of the Seed and Idriss (1970) curves were considered as reference. A frequency independent expression [i.e. $G^* = G\,(1+2iD)$] was adopted for the complex formulation of the shear modulus, while the effective shear strain ratio (R) was set at 0.65, which is commonly adopted in EL analyses as the multiplier of the maximum shear strain to obtain an effective shear strain [i.e. $\gamma_{\mathrm{eff}} = R\,\gamma_{\mathrm{max}}$] that is considered as more representative of the shear strain time history at a specific depth. It is noted that for the first 1.5 m of the soft NC clay profile, constant values for the low-strain shear modulus and the undrained shear strength at 2.55 MPa and 6.2 kPa, respectively, were considered due to a numerical issue observed in DEEPSOIL when very low values of the above parameters are introduced. Below 1.5m, the s_u and the G_0 profiles follow the linear variation with depth described by Equations 9 and 11, respectively. For the non-linear (NL) analyses in time domain, the General Quadratic/Hyperbolic (GQ/H) model (Groholski et al. 2015) implemented in DEEPSOIL was adopted to model the backbone curve of the shear stress-strain relationship. The GQ/H model allows the shear strength of the soil to be directly introduced as an input parameter, contrary to the Modified Kondner Zelasko (MKZ) model (Matasovic 1993), which may overestimate the shear strength of the soil depending on the values of the curve-fitting parameters (Groholski et al. 2016). For the hysteretic soil behaviour during unloading and reloading, the associated stress-strain loops were defined on the basis of the non-Masing Modulus Reduction and Damping with reduction Factor (MRDF) formulation proposed in Phillips and Hashash (2009), to avoid damping overestimation at large shear strains when Masing rules are adopted (Kwok et al. 2007). Curve fitting was performed for a range of γ up to 0.1% under the hypothesis that the shear stresses reach 95% of the shear strength at a 10% shear strain, while the value of the model parameter θ_3 was fixed at unity, as suggested in Groholski et al. (2016).

The 3D Finite-Difference (FD) soil-pile model in FLAC3D

The 3D FD soil – pile model in FLAC3D employed herein is shown in Fig. 3, following a sensitivity analysis on critical modelling aspects such as model size, discretization scheme, pile and pile-soil interfaces modelling (see electronic supplement). Thus, only the main attributes of the 3D model are given in the ensuing.

The soil-pile model has a base, width, and height equal to 30m, 30m, and 31m, respectively. The one-meter-thick bottom layer was used to model the elastic bedrock with a shear wave velocity of

800 m/s and a unit weight equal to 22 KN/m^3. The grid-element size in the vertical direction (z-axis) was selected according to the indications provided in Kuhlemeyer and Lysmer (1973), where it is suggested that for an accurate representation of wave transmission through a model, the element size, must be smaller than 1/8 of the wavelength associated with the highest frequency component of the input wave. Considering the stiffness profiles of the sand and OC Clay soils, the thickness (h_i) of the soil elements was selected in these cases equal to 0.50m from ground surface down to 20m and 1.0m between 20m and the bottom of the model. For the soft NC clay profile, the first 20 m were discretized with 80 layers of 0.25 m thickness each, while 20 layers of 0.50 m thickness each were adopted to discretize the soil profile between 20 – 30 m. The same discretization was adopted in the DEEPSOIL code. In this manner, a minimum $f_{max,i}$ at 40 Hz is considered which is quite above the value of $f_{max,i}$ = 25 Hz recommended by Hashash et al. (2016). Note that $f_{max,i}$ (= $V_{s0,i}$ / 4H_i) refers to the maximum frequency that a layer of thickness H_i and of shear wave velocity $V_{s0,i}$ can propagate. A linear elastic behaviour is assumed for the pile material.

Nonlinear soil response was accounted for via the *sig3* hysteresis model (Itasca, 2017) for the Sand and OC clay profiles, and via the *UCSDCLAY* model (Elgamal et al. 2008) for the NC clay. The *UCSDCLAY* model is a pressure-independent 3D elasto-plastic material model, which enables reproducing nonlinear hysteric shear behavior, and it was preferred over the *sig3* model because it allows the shear strength of the soil to be introduced as a direct input. Rayleigh damping, which is commonly applied to take into account small strain (viscous) damping or to remove high frequency noise, was found to be unnecessary. *Sig3* and *UCSDCLAY* model parameters are described in the electronic supplement.

No interface elements were introduced between soil and pile, following a relevant sensitivity analysis under kinematic loading (see electronic supplement). In this regard, pile-head bending moments were compared between soil-pile models with and without consideration of interface elements that are available in FLAC3D and they are characterized by Coulomb sliding and/or tensile and shear bonding. The above sensitivity analysis that was performed for various soil-pile configurations and input motions revealed a minor effect of the interface elements on pile's kinematic response and therefore perfect bonding between soil and pile elements was assumed during the parametric study reported in the following. Such an assumption is in line with earlier analytical findings, which indicate that soil-pile contact stresses under kinematic loading are quite lower compared to those induced by forces or moments applied at the pile-head, while the kinematic-induced contact stresses show a weak dependence on pile diameter (Di Laora et al. 2017). The above difference between kinematic- and inertial-induced contact stresses, stemming from the associated deviation of the corresponding relative displacements between soil and pile, was also verified in the framework of the present study (see electronic supplement).

In the dynamic analyses, free-field boundaries were imposed at the lateral end-nodes of the main grid of the model (Fig. 3). Free-field boundaries in FLAC3D consist of four column grids and four plane grids located at the corners and side boundaries of the model, respectively (Fig. 3). Soil behaviour in these free-field zones follows the same constitutive law as in the main grid. Quiet absorbing (viscous) boundaries were applied at the base of the model, so that the downward-propagating waves cannot be reflected back in the soil mass. In the same spirit, the lateral boundaries of the main grid are connected through viscous dashpots with the free-field grid, which simulate a quiet boundary to absorb the waves radiated from the pile motion. In this manner, the free-field grid executes the same motion as the main grid. Further details on FLAC3D free-field boundaries formulation can be found in Itasca (2017). The dynamic loading was applied at the base of the model in the form of a shear stress time history.

NC Clay model calibration

In order to obtain a meaningful comparison of the free-field soil response between DEEPSOIL and FLAC3D codes, a recursive calibration procedure was followed to obtain similar non-linear behaviour between the associated soil models, GQ/H and USCDCLAY, respectively. For the most sensitive case of the NC Clay this procedure was composed of the following steps (Fig. 4): (i) first, the GQ/H model was calibrated by the Vucetic and Dobry (1991) curves for I_p = 40% (noted in Fig. 4 as DS fit.1), (ii) the fitted DEEPSOIL curves were employed to calibrate the USCD Clay model introduced in FLAC3D and (iii) the fitted FLAC3D-based curves were employed to calibrate again the GQ/H model (noted in Fig. 4 as DS fit.2). In this manner, it was possible to derive comparable $\tau - \gamma$ backbone curves between the two codes (Fig. 4c) at the expense of higher hysteretic damping at large strains with respect to the experimental data (Fig. 4b). The corresponding calibration of the *sig3* model employed in FLAC3D for the sand and the OC Clay soils is reported in the electronic supplement.

FREE-FIELD GROUND RESPONSE

Free-field ground response under the prescribed input motions was first derived with DEEPSOIL code by implementing the EL and NL models described above. Fig. 5 and 6 compare EL and NL analyses results for the OC Clay and the NC Clay profile, respectively, in terms of peak ground acceleration (Fig. 5a, 6a), maximum shear strain (Fig. 5b, 6b) and maximum shear stress (Fig. 5c, 6c) profiles, referring to average values between those computed separately for each one of the seven base excitations. An effective shear strain profile was then computed as 0.65 times the maximum strain developed at any depth, which in turn was employed to obtain the corresponding mobilized shear modulus and damping profiles based on the calibrated $G/G_0 - \gamma - D(\%)$ curves. In this manner a single mobilized stiffness and damping profile was derived for each one of the seven input motions. An average mobilized G obtained by averaging these seven profiles is shown in Fig. 5d and 6d for the OC Clay and the NC Clay profile, respectively. It is noted that all the results shown in Fig. 5 and 6 correspond to the maximum PRA considered at 0.25g. Ground response analysis results for the NC clay profile when PRA is considered at 0.10g and 0.15g, are given in the electronic supplement.

With reference to the stiffer OC Clay profile, EL and NL analyses result in comparable soil response, which is reasonable since the average shear strains are below the threshold values of the equivalent linear approximation. The behavior of the soil is far from failure (Fig. 5c) and, therefore, it is mainly controlled by its stiffness. A similar response was observed for the sand profile, resulting in even lower values of maximum shear strains in the order of 0.04 %. On the contrary, for the soft NC Clay (Fig. 6), the EL approximation is not able to capture the complex soil behaviour. Indeed, under the EL assumption, a sudden increase of the peak ground acceleration is observed close to the ground surface, being in qualitative agreement with analytical elastodynamic investigations reported in Rovithis et al. (2011) for a similar shear wave velocity profile. However, under NL considerations, ground acceleration is de-amplified as it propagates through the soil due to the low shear strength of the soft clay, which limits the transmission of shear stresses.

Similar findings on the seismic behavior of soft clays are reported in relevant experimental studies (Afacan et al. 2013; Zhou et al. 2017; Garala and Madabhushi 2019). In further support to the above, the τ-γ loops derived at two depths close to the ground surface, where soil properties dominate kinematic interaction, are plotted in Fig. 7 under the most intense loading (i.e. PRA = 0.25g). The strong non-linear behavior of the soil generates large inelastic strains on the order of 1%, while the developed shear stresses are bounded by the low shear strength s_u of the soft clay. Apparently, such a complex soil response cannot be captured by the EL approximation as evident by the corresponding linear elastic τ-γ relationship shown in Fig. 7, which indicates that the shear stress and strain are in-phase and proportional to each other. This does not mean absence of energy dissipation through the hysteretic behavior of the soil, as the latter is taken into account through the complex shear modulus during each iteration of an EL analysis.

The corresponding average profiles of free-field ground response obtained with FLAC3D are also plotted in Fig. 5 and 6. It is noted that soil response in FLAC3D is retrieved from the grid-points at the side boundary of the main grid (Fig. 3). It is observed that when the level of the shear strain allows consideration of the EL approximation like in the case of OC Clay (Fig. 5), the response profiles obtained by the two codes almost coincide. For larger levels of shear strain mobilizing strong non-linear soil behavior like in the case of NC Clay (Fig. 6), the agreement is still encouraging between DEEPSOIL NL and FLAC3D analysis, allowing critical trends of ground response, such as the de-amplification of acceleration under strong shaking, to be similarly reproduced. The above provides confidence that the adopted model in FLAC3D is able to reproduce highly non-linear ground response and, therefore, kinematic soil-pile interaction over a wide range of shear strains.

KINEMATIC PILE-HEAD BENDING

Upon considering that there is an effective portion of the soil controlling pile-head bending, which is proportional to a characteristic wavelength of the soil-pile system, Di Laora and Rovithis (2015) introduced the notion of an effective soil curvature $(1/R)_{s,eff}$ [= $\gamma_s(z_{eff})$ / z_{eff}] to derive a simple analytical expression for the kinematic bending moment at the head of a pile in a continuously inhomogeneous soil. In the above definition, the depth z_{eff} is considered as one half of the pile's active length L_a and $\gamma_s(z_{eff})$ is the corresponding shear strain of soil at z_{eff}.

Derivation of the effective depth z_{eff}

In the general case of an inhomogeneous soil profile with shear stiffness varying continuously with depth according to the law:

$$G_s(z) = G_{sd}\left[a + (1-a)\frac{z}{d}\right]^n \tag{13}$$

where $G_s(z)$ is the depth-varying soil shear modulus, G_{sd} is the shear modulus at the depth of one pile diameter (i.e., at $z = d$) and a, n are dimensionless factors controlling the stiffness profile, the active length of the pile may be calculated by the expression (Di Laora and Rovithis 2015; Karatzia and Mylonakis 2016, Iovino et al. 2019):

$$L_a = \frac{d}{1-a}\left\{\left[a^{\frac{n+4}{4}} + \frac{5}{16}(n+4)(1-a)\left(\frac{\pi}{2}\frac{E_p}{E_{sd}}\right)^{\frac{1}{4}}\right]^{\frac{4}{n+4}} - a\right\} \tag{14}$$

where E_{sd} is the Young's modulus of elasticity of the soil at one pile diameter depth.

At this point one has to fit the mobilized shear modulus profile derived from 1D ground response analysis, to the formula of $G_s(z)$ in Equation 13 in order to obtain the parameters G_{sd}, a and n and then calculate L_a from Equation 14 and z_{eff} as (Di Laora and Rovithis 2015):

$$z_{eff} = L_a/2 \tag{15}$$

As the above parameters are interrelated, an iterative procedure may be followed by considering the value of $L_a = 10d$ as a starting point and employing a least squares linear (i.e. $n = 1$) fit. To this end, a single iteration leads to quite accurate results. Representative results of the fitting procedure for the mobilized shear modulus profile obtained with FLAC3D at free-field conditions under the Nahanni record scaled to PRA = 0.25g are shown in Fig. 8 for each one of the three soil profiles under consideration.

Analytical formula revisited for highly nonlinear soil response

Under constant ground acceleration, a_s, Di Laora and Rovithis (2015) proved that the ratio of the pile-head curvature $(1/R)_p$ over $(1/R)_{s,eff}$ for long piles is equal to 1, which allows calculation of pile-head kinematic bending by the formula:

$$M_{kin} = \mathrm{E_p I_p}(1/R)_p = \mathrm{E_p I_p}(1/R)_{s,eff} = \mathrm{E_p I_p}\frac{\gamma_s(z_{\mathrm{eff}})}{z_{\mathrm{eff}}} \tag{16}$$

A simple expression for short piles is also proposed in the above study. The equilibrium of a 1D soil column with constant mass density ρ_s and variable shear modulus $G(z)$ with depth yields that $\gamma(z_{eff})$ may be expressed as:

$$\gamma_s(z_{\mathrm{eff}}) = \frac{a_s \rho_s z_{\mathrm{eff}}}{G(z_{\mathrm{eff}})} \tag{17}$$

where $G(z_{eff})$ is the mobilized shear modulus of the soil at z_{eff}. Upon introducing the above expression in Equation 16 one gets:

$$M_{kin} = \mathrm{E_p I_p}\frac{a_s \rho_s}{G(z_{\mathrm{eff}})} \tag{18}$$

The performance of Equations 16 and 18 is compared with the 3D Finite-Difference model response, in the form of the ratio $M_{\mathrm{kin,formula}}$ / $M_{\mathrm{kin,FLAC3D}}$ for all the examined combinations of soil profiles and input motions scaled to 0.10g, 0.15g and 0.25g (Fig. 9). Each group of bars refers to a different base excitation noted in the abscissa of the plots. More specifically, Fig. 9a, 9c and 9e show the predictions of Equation 16 while Fig. 9b, 9d and 9f refer to those of Equation 18. To this end, the maximum shear strain $\gamma_{\mathrm{max,s}}(z_{\mathrm{eff}})$ at z_{eff} was introduced in Equation 16, while the peak ground acceleration at soil surface was employed to derive $M_{\mathrm{kin,formula}}$ by means of Equation 18. Both of these parameters were obtained by the FLAC3D model response for the purpose of this comparison.

It is observed that up to strain levels which allow modelling of the soil behaviour by the equivalent linear approximation, such as those generated in the case of the sand and the OC clay profiles, both formulae provide good predictions of kinematic pile-head bending, leading to ($M_{\mathrm{kin,formula}}$ / $M_{\mathrm{kin,FLAC3D}}$) ratios close to unity. Understandably, the above is more obvious for the case of the sand layer (Fig. 9a and 9b), where the lowest $\gamma_{\mathrm{max}}(z_{\mathrm{eff}})$ was generated at z_{eff} with respect to the other two soil profiles.

On the contrary, for the NC Clay profile, where the maximum shear strain at z_{eff} attains considerably larger values up to 0.8 - 1 %, the kinematic pile-head bending predicted by Equation 16 is much closer to the FD solution (Fig. 9e), denoting that the maximum shear strain at z_{eff} is a better indicator of the developed pile-head bending compared to ground surface acceleration (Fig. 9f), when soil behaviour is close to failure. However, despite its better performance, Equation 16 may still be quite conservative for certain geotechnical conditions and base excitations, like in the case of the NC Clay profile where an average overestimation of 30% is observed, while the deviation is maximized at approximately 50% under the Whittier base motion (Fig. 9e).

Frequency effects

This over-prediction of the kinematic bending is explainable, though, as it follows the original conservative assumption of constant ground acceleration to derive Equation 16, implying low-frequency excitations. This means that Equation 16 may be viewed as an upper bound of the kinematic bending moment, which is valid when the frequency content of the time variant parameter $\gamma_s(z_{eff})$ controlling the kinematic demand is low enough to be considered as almost statically applied. If the above assumption is not accurate, the bending moment attains lower values as the shear strain (and the corresponding effective soil curvature) is a decreasing function of the excitation frequency regardless of the soil properties (Di Laora and Rovithis 2015).

Frequency effects may, thus, be taken into account by means of the dimensionless frequency $a_{\mathrm{eff,La}}$ which controls the kinematic response of the pile in the dynamic regime (Di Laora and Rovithis 2015; Iovino et al. 2019):

$$a_{eff,La} = \frac{\omega L_a}{V_{s,av}} \tag{19}$$

where ω is the cyclic frequency of the excitation, L_a is the active length of the pile and $V_{s,av}$ refers to an average shear wave velocity within z_{eff} given by:

$$V_{S,av} = V_{Sd}(L_a/4d)(a-1)(n-2)\left[\left(a+(1-a)\frac{L_a}{2d}\right)^{1-n/2} - a^{1-n/2}\right]^{-1} \tag{20}$$

In the above expression, V_{sd} is the mobilized shear wave at one pile diameter depth, which may be derived by the corresponding value of G_{sd} once the mobilized shear modulus profile is fitted to a linear function as suggested earlier. Then, consideration of frequency effects in kinematic bending is possible by implementing the expression of the dynamic $(1/R)_{\mathrm{p,dyn}}$ over the static $(1/R)_{\mathrm{p,static}}$ pile curvature ratio proposed in Di Laora and Rovithis (2015):

$$(1/R)_{p,dyn}/(1/R)_{p,static} = [1 + 0.02a_{eff,La}^3]^{-1} \tag{21}$$

which is a continuous function of ω. To obtain a single-valued prediction of the kinematic pile-head moments in the dynamic regime, we consider a mean cyclic frequency $\omega_{m,\gamma}$, as an index of the frequency content of the shear strain time history at z_{eff}, since $\gamma_s(z_{\mathrm{eff}})$ was proven to control the kinematic pile-head bending at higher strains. Following the definition of the mean period (T_{m}) of an acceleration time history introduced in Rathje et al. (1998), $\omega_{\mathrm{m},\gamma}$ may be computed from:

$$\omega_{m,\gamma} = 2\pi \frac{\sum_i C_{i,\gamma}^2}{\sum_i C_{i,\gamma}^2 \left(\frac{1}{f_i}\right)} \qquad (22)$$

where $C_{\mathrm{i},\gamma}$ refer to the Fourier amplitudes of the shear strain time history at z_{eff} and f_{i} are the discrete Fourier transform frequencies between 0.25 Hz and 20 Hz.

In this manner, a mean dimensionless frequency $a_{\mathrm{eff,m,La}}$ of the shear strain demand at z_{eff} may be defined by introducing $\omega_{\mathrm{m},\gamma}$ in Equation 19:

$$a_{eff,m,L_a} = \frac{\omega_{m,\gamma} L_a}{V_{s,av}} \qquad (23)$$

where L_{a} and $V_{\mathrm{s,av}}$ may be computed by the analytical expressions in Equations 14 and 20, respectively, based on the linear fit of the actual mobilized soil stiffness profile. Alternatively, $V_{\mathrm{s,av}}$ can be derived as the harmonic mean of the mobilized shear wave velocity profile between ground surface and z_{eff} (= L_{a} / 2), which is adopted herein. Upon introducing $a_{\mathrm{eff,m,La}}$, Equation 21 is rewritten as:

$$(1/R)_{p,dyn}/(1/R)_{p,static} = [1 + 0.02 a_{eff,m,L_a}^3]^{-1} \qquad (24)$$

which now allows a single value of the $(1/R)_{\mathrm{p,dyn}}$ / $(1/R)_{\mathrm{p,static}}$ ratio to be derived for each combination of soil profile and base excitation according to the associated value of $a_{\mathrm{eff,m,La}}$. It is reiterated that for long piles, $(1/R)_{\mathrm{p,static}} = (1/R)_{\mathrm{s,eff}}$. Upon combining Equations 16 and 24, kinematic bending at the pile-head, including frequency effects, can be expressed as:

$$M_{kin} = \mathrm{E_p I_p} \frac{\gamma_{max,s}(z_{\mathrm{eff}})}{z_{\mathrm{eff}}} [1 + 0.02 a_{eff,m,L_a}^3]^{-1} \qquad (25)$$

The performance of the above expression against the FD results is shown in Fig. 10 for each soil profile under consideration. The improvement of the agreement between the two solutions with respect to that shown in Fig. 9a, 9c and 9e cannot be overstated, denoting maximum deviations in the order of 10% or less, even for the NC Clay profile. This proves that in the latter case, the assumption of low-frequency loading was conservative, leading, accordingly, to an over prediction of the FD-based pile bending, when frequency effects are disregarded. More importantly, the agreement in Fig. 10 suggests that the simple analytical formula in Equation 25 is applicable even in the highly nonlinear range of soil response close to failure, provided that the associated maximum shear strain demand induced by the surrounding soil and the corresponding mobilized stiffness profile are introduced. It may thus be asserted that dynamic effects result in modifying solely soil deformations at free-field conditions while soil-pile kinematic interaction mechanism remains static. In other words, the dynamic nature of kinematic pile bending stems from the superposition of a dynamic phenomenon, referring to ground response under earthquake shaking and a static problem related to pile-soil interaction. This interpretation was first discussed by Di Laora et al. (2012) for homogeneous soils and confirmed further in Di Laora and Rovithis (2015) for nonhomogeneous soils. The results of this study extend, therefore, the validity of the simple analytical solutions to the non-linear range of soil response, denoting that kinematic soil-pile interaction is controlled by the soil stiffness even if the response of the soil itself is controlled by its strength. The above finding generalizes earlier indications (Mucciaciaro and Sica 2018, Stacul and Squeglia 2020, Garala et al. 2020) of the controlling role of the mobilized soil stiffness on pile kinematic bending.

It is reiterated that all the above analytical derivations were performed by introducing the free-field ground response parameters computed from the FLAC3D model analyses in the time domain. In this manner, the free-field demand imposed on the pile by the surrounding soil was compatible to the reference pile-head bending moments, in the sense that they were both derived from the same numerical model. Of course, if the kinematic demand imposed by the surrounding free-field soil was derived by a different code oriented for ground response analysis, like DEEPSOIL employed herein, the resulting bending moments could be, accordingly, different, but only due to the modification of ground response; not due to the interaction problem. This means that the revisited analytical formulae allow the derivation of kinematic pile-head bending by performing only a 1D free-field ground response analysis with a proper constitutive model to describe soil behaviour for the problem at hand and subsequently by fitting the mobilized stiffness profile with a linear function to derive L_a, z_{eff}, and $a_{eff,m,La}$. Such an independent derivation of the free-field ground response may even be suggested when the constitutive law models better experimental data (Fig. 4b). Further support on the above is provided by the analysis of a real soil profile reported in the ensuing, following a general work-flow that provides guidance to assess kinematic pile response in design.

PILES FILTERING ACTION

To quantify the filtering potential of piles, reference is made to the ratio (I_u) between the pile-head horizontal displacement (or acceleration) over the free-field horizontal displacement at the ground surface (or acceleration). A novel physical interpretation of the filtering effect is reported in Iovino et al. (2019), based on the concept that a portion of the pile, being a fraction of its active length, averages, due to its stiffness, the displacement field imposed by the surrounding soil. As the wavelength in the soil decreases with respect to this portion of the pile, the average soil displacement is reducing and, accordingly, I_u decreases. The latter also holds if the frequency of excitation increases under constant pile diameter, pile stiffness and soil stiffness. On the other hand, for a given excitation frequency, I_u decreases with increasing pile diameter and Young's modulus and with decreasing soil stiffness, indicating that the investigation of the filtering action becomes meaningful especially in the case of stiff and large-diameter piles in soft soils; a soil-pile configuration which may also trigger large kinematic bending, as shown above.

Harmonic response

Iovino et al. (2019) proposed the following simplified expression for I_u:

$$I_u = \begin{cases} \left[1 + 0.02\, a_{eff,La}^3\right]^{-1} & for\ a_{eff,La} < 5 \\ 0.29 & for\ a_{eff,La} \geq 5 \end{cases} \tag{26}$$

under the assumption of a linear viscoelastic soil model, where $a_{\mathrm{eff,La}}$ is given by Equation 19. In this study, the applicability of Equation 26 is explored when large shear strain levels are attained in the soil, in the same spirit as the investigation performed earlier for kinematic pile-head bending.

Fig. 11 and 12 compare numerically obtained I_u curves between nonlinear time domain analyses with FLAC3D and equivalent linear frequency domain analyses with ANSYS FE code v.15 (Ansys Inc. 2005), for PRA = 0.10g and 0.25g, respectively. The performance of the simplified expression in Equation 26 is also plotted. Each I_u curve shown in Fig.11 and 12 corresponds to the average of seven obtained for each one of the input motions. It is noted that ANSYS analyses were performed by modeling the exact distribution of the mobilized shear modulus [$G_{mob}=G(0.65\gamma_{max})$] and damping ratio [$D_{mob}=D(0.65\gamma_{max})$] with depth, derived from the nonlinear analyses with FLAC3D for each input motion. For the implementation of the simplified formula, $a_{eff,La}$ was computed for each input motion by means of Equation 19, following the linear fit of the mobilized stiffness profile at free-field conditions derived from FLAC3D. The agreement between the three modeling considerations is quite satisfactory, with the exception of the NC Clay, where the simplified solution underestimates I_u above 1.5 Hz approximately. This should be attributed to the associated linear fit, which is not able to reproduce in a precise manner the actual distribution of the mobilized shear modulus at shallow depths (Fig.8). On the other hand, the close agreement between FLAC3D and ANSYS analyses results over the whole frequency range and for all the examined soils (including the NC clay), provides further support on the proposed equivalent-linear approximation of kinematic interaction, while it indicates that soil properties close to the ground surface (i.e., approximately down to 5 pile diameters in depth) rule the filtering effect.

Time-domain response

A practical application of I_u lies on the derivation of the pile-head acceleration, a_p(t), in time domain by means of Fourier (FFT) and inverse Fourier (iFFT) transformations involved in the following expression:

$$a_p(t) = iFFT[I_u(\omega) * FFT(a_s(t))] \tag{27}$$

where a_s(t) stands for the acceleration time history at the free-field ground surface. Having computed a_p(t), a mean spectral acceleration ratio ξ, which is defined as the ratio between the average response spectrum of the pile-head motion ($S_{a,p,av}$) over the average response spectrum of the free-field motion ($S_{a,s,av}$), may be derived as a means to quantify piles filtering effect on free-field motion. To this end, the pile-head and free-field surface acceleration response spectra were computed for each one of the seven input motions and were then averaged to derive the mean spectral acceleration ratio ξ.

Fig. 13 and 14 compare ξ between FLAC3D analyses, ANSYS analyses and the simplified procedure (Equations 26 and 27) for PRA at 0.10g and 0.25g, respectively. It is observed that the simplified procedure allows the assessment of the filtering action of piles for the Sand and OC clay soils, while the large deviation in the case of the NC Clay soil follows the similar trend observed in the frequency domain as a result of the linear fit of the actual mobilized stiffness profile. This is again confirmed by the closer agreement between FLAC3D and ANSYS results, which strengthens the assertion of an equivalent linear kinematic interaction, even at large shear strains close to soil failure.

As a final comment, Fig. 15 shows the average amplitude of I_u superimposed to the average spectral ratio obtained for PRA = 0.25g, against $1/f$. It is observed that the periods at which both ξ and I_u attain local minimum practically coincide for each one of the examined soil profiles, which is reminiscent of the similar finding reported in Iovino et al. 2019 for linear soil behavior. This means that the period corresponding to maximum filtering is independent of the input motion characteristics, also in the non-linear regime.

CASE STUDY: ANALYSIS OF A REAL SOIL PROFILE

Assessment of kinematic effects was further explored upon considering a fixed-head elastic pile embedded in a layered site in the Po plain region of Northern Italy. In this case, a larger range of parameters was considered by implementing two pile diameters (*d*) at 1 m and 1.5 m, while the elastic properties and the length of the pile was considered the same as before. Following a large geotechnical investigation of the site, reported in Licata et al. 2019 and Conti et al. 2020, the particular soil profile is formed by approximately horizontal layers and it is composed of a 5 m thick made ground (MG) followed by very soft clayey silts (CS) up to 20-25 m from the ground surface. A 2 m thick peat layer (P) is interbedded at the level of 14 m. Then, alternating layers of silty sands and sandy silts (SS) are met between 25 to 30 m approximately, which are underlain by stiffer clayey silts. The physical and mechanical properties of the above soil layers are presented in Table 2 until the elevation of 100 m, where the seismic bedrock (V_s = 800 m/s, γ = 20 kN/m^3) is considered. The $G - \gamma$ (%) – D (%) curves of each soil type are shown in Fig. 16. Further information on site properties can be found in the above references.

Kinematic pile-head bending moments and pile's filtering action were derived under the same input motions (Fig.2) imposed at the base of the soil profile and scaled to the same PRA values (0.10g, 0.15g and 0.25g).

Assessment of pile-head kinematic moments and pile filtering action

Free-field response of the layered soil profile was first obtained by FLAC3D and DEEPSOIL upon implementing the non-linear constitutive laws for soil behavior that were described above during the analysis of the three idealized soil profiles. Maximum shear strain and mobilized shear modulus profiles obtained from DEEPSOIL analysis are presented in Figs. 17a and 17b, respectively, for PRA at 0.15g. A linear fit was then performed to each mobilized stiffness profile within the active length of the pile for each one of the two pile diameters under consideration. Understandably, increasing pile diameter will provide a larger active length. Representative results of the linear fit are shown in Fig.17c under for the Coyote input motion scaled to 0.15g. In this case, the iterative procedure resulted in an active pile length at 7.11 m and 10.47 m for pile diameter d at 1.0 m and 1.5 m, respectively. Accordingly, z_{eff} was computed at 3.56 m and 5.24 m by means of Equation 15.

For each combination of input motion, PRA and pile diameter, maximum kinematic pile-head moments were computed by introducing in Equation 25: (i) the maximum shear strain $\gamma_{\max}(z_{\mathrm{eff}})$ at z_{eff} and (ii) the frequency reduction factor (Equation 24) involving the mean cyclic frequency $\omega_{\mathrm{m},\gamma}$ of the shear strain time history at the same elevation. $V_{\mathrm{s,av}}$ was derived again as the harmonic mean of the mobilized shear wave velocity profile along z_{eff}. The above calculations were made on the basis of free-field response computed from both DEEPSOIL and FLAC models and the predictions of Equation 25 were compared with the FD results obtained from the time domain analyses of the 3D soil-pile model in FLAC. The comparative results are plotted in Figs.18a and 18b for pile diameter at 1 m and 1.5 m, respectively. In these plots, ground response parameters introduced in Equation 25 were obtained from DEEPSOIL NL analyses. Similarly, Figs 19a and 19b refer to the case when ground response parameters introduced in Equation 25 were obtained from FLAC analyses. The deviation in the agreement that is observed especially between Fig.18a and Fig. 19a (d = 1 m) should not come as a surprise, as it follows the deviation in free-field response parameters between the two soil response analyses. This is supported by the comparison of maximum shear strain at z_{eff} between DEEPSOIL NL and FLAC analyses shown in Figs. 20a and 20b for d = 1 m and d = 1.5 m, respectively. Indeed, for z_{eff} corresponding to d = 1 m, there is a considerable deviation of $\gamma_{\max}(z_{\mathrm{eff}})$ between DEEPSOIL and FLAC analyses, which is reflected in the deviation of pile-head bending moments shown in Fig. 18a. On the contrary, for the larger z_{eff} corresponding to d = 1.5 m, the values of $\gamma_{\max}(z_{\mathrm{eff}})$ are comparable, which is accordingly reflected in the correlation of bending moments shown in Fig.18b. Apparently, the predictions of the formula when the FLAC-based ground response parameters are introduced follow closer the FD results (Figs 19a and 19b) as both of them were retrieved from the same numerical model. However, mention has already been made that an independent derivation of the free-field ground response combined with Equation 25may even be suggested, when the constitutive law models better experimental data, which is actually true in this case. Indeed, the constitutive law employed in DEEPSOIL seems to capture better the nonlinear behavior of the soil, as shown in the stiffness degradation and damping curves compared in Fig. 21 between experimental data, DEEPSOIL model-fitted curves and FLAC model-fitted curves. Support on the better predictive capability of this simplest approach (i.e. application of Equation 25 by means of the ground response parameters from DEEPSOIL) even over the complex numerical analyses seems to come from the fact that the revisited formula (Equation 25) describing the interaction mechanism has slightly lower scatter with numerical results (Fig. 19) compared to the difference between FLAC and DEEPSOIL ground response (Fig. 20).

The applicability of the proposed procedure for the real soil profile under study was then tested in terms of the filtering action exerted by the pile. Fig. 22 compares FLAC3D results with Equation 26 predictions of average I_u for d = 1 m (Fig. 22a) and d = 1.5 m (Fig. 22b). To this end, L_a and $V_{s,av}$ introduced in the formula of the dimensional frequency $a_{eff,La}$ (Equation 19) were computed for each input motion, based on the linear fit of the corresponding mobilized shear modulus profile obtained from free-field ground response analysis using both DEEPSOIL non-linear and FLAC3D models. The same comparisons in terms of the average spectral acceleration ratio ξ are shown in Fig. 23 for d = 1 m (Fig. 23a) and d = 1.5 m (Fig. 23b). All plots in Figs. 22 and 23 refer to PRA = 0.15 g. Understandably, higher filtering action is exerted by larger diameter piles as it is reflected in the lower values of I_{u} and minimum ξ derived for d = 1.5 m. Again, the small deviations observed between the ξ curves in Fig. 23 should be attributed to the different free-field acceleration at ground surface (Equation 27) between FLAC and DEEPSOIL, and not to the inability of the formula to describe the interaction mechanism.

CONSIDERATION OF PILE NONLINEARITY

So far, kinematic effects were explored under the hypothesis of linear elastic pile behaviour. However, it is possible to consider also the non-linear behaviour of the pile by introducing an effective pile stiffness being compatible to a given moment – curvature relation. To this end, further analyses were carried out via the boundary element method (BEM) code KIN SP (Stacul and Squeglia, 2018, 2020), where the bending moment - curvature (M - ψ) relation of the pile section can be approximated with a bilinear model. The general rules to model the nonlinear pile response with KIN SP are: (i) in the uncracked stage (i.e., $M < M_{cr}$, where M_{cr} is the cracking moment) the flexural stiffness is the intact flexural stiffness $(E_pI_p)_{uncracked}$; (ii) once the bending moment exceeds M_{cr}, the cracked flexural stiffness $(E_pI_p)_{cracked}$ is assigned to the cracked section. The latter is equal to $(M_y\text{-}M_{cr})/(\psi_y\text{-}\psi_{cr})$, where ψ_{cr} is the curvature at M_{cr}, while M_y and ψ_y refer to the moment at the first bar yielding and the corresponding curvature, respectively; (iii) the post-cracking unloading/reloading paths are ruled via the secant flexural stiffness $(E_pI_p)_{sec} = M_{rev}/\psi_{rev}$, where M_{rev} and ψ_{rev}, are the maximum bending and the corresponding curvature attained at the pile section at the reversal point, respectively. The pile in KIN SP is assumed to be embedded in a multilayered half space, where the mobilized shear modulus coming from free-field soil response analysis is assigned to each soil layer.. It is noted that free-field soil response obtained with KIN SP (not shown here) was compared against numerical results from FLAC analyses and a good agreement was observed between the two models. The pile is forced with the soil displacement and velocity time histories obtained from the free-field analysis at each soil layer and the kinematic interaction analysis is performed in the time domain. Further details are available in the above references.

Kinematic effects accounting for pile nonlinear behaviour were explored for the complete set of soil-pile configurations analysed above under linear pile behaviour, extending the investigation for different steel reinforcement ratios. Thus, 4 soil profiles, 7 input motions, 3 levels of PRA (0.1g, 0.15g and 0.25g), 2 pile diameters (d = 1.0 m, 1.5m) and 4 steel reinforcement ratios (A_s/A_c = 0.5%, 1%, 2% and 4%) were considered, for a total of 672 pile-soil-earthquake configurations.

The intact flexural stiffness of the pile section, $(E_pI_p)_{\mathrm{uncracked}}$, was kept equal to that considered in the analyses where the pile was assumed to behave in a linear elastic manner. The cracking moment (M_{cr}), the cracked flexural stiffness, $(E_pI_p)_{\mathrm{cracked}}$, the moment at first bar yielding (M_y) and the ultimate moment of the section (M_{ult}) were defined considering the Mander et al. (1988) model for the confined concrete in compression (f_c = 25 MPa, E_c = 25 GPa), the Popovics (1973) model for the unconfined concrete in compression, the CEB-FIP (1993) model for the concrete in tension and a simple bilinear model for the steel reinforcement (E_{steel} = 210 GPa, $f_{s,y}$ = 450 MPa, $f_{s,t}$ = 540 MPa). Tables 3 and 4 summarize the pile section properties used in the kinematic interaction analyses.

The results obtained via KIN SP have been used for developing an additional simplified procedure to take into account for the nonlinear response of the pile section. As (E_pI_p), L_a, z_{eff}, $\gamma_{\max,s}(z_{\mathrm{eff}})$ and the resulting kinematic bending moment at the pile head M_{kin} (Equations 14, 15 and 16) are interrelated, the application of the above formula in the pile nonlinear regime (i.e when M_{kin} is larger than M_{cr}) may be performed by an iterative procedure, where an effective flexural stiffness of the pile, $(E_pI_p)_{\mathrm{eff}}$, is updated in each iteration according to the following formula:

$$\left(\mathrm{E_pI_p}\right)_{eff} = \alpha \frac{M_{kin}}{\psi_{kin}} \tag{28}$$

where the dimensionless parameter α accounts for the fact that from $z = 0$ to $z = L_a$ only a portion of the pile shaft will experience bending moments larger than M_{cr}. Upon updating $(E_pI_p)_{\mathrm{eff}}$, new values for L_a, z_{eff}, $\gamma_{\max,s}(z_{\mathrm{eff}})$ and eventually M_{kin} are derived. Once the updated value of M_{kin} is obtained, the corresponding curvature ψ_{kin} and the secant flexural stiffness (M_{kin}/ψ_{kin}) of the pile section are evaluated via the (M - ψ) relation. By implementing the above iterative process and evaluating α values which permitted to obtain the best fit with the numerical results, the following empirical formula was established for the dimensionless factor α:

$$\alpha = 1 + 7\left(\frac{M_{kin}}{M_{ult}}\right)^{2.5} \tag{29}$$

for the bilinear (M - ψ) relation under consideration. However, more sophisticated moment – curvature relationships including also the effect of the pile's axial load (considered zero herein) may be equally adopted within the above iterative framework of analysis. Once convergence is attained, the kinematic bending moment at the pile head should be corrected to take into account also the frequency effects via Equation 24. Fig. 24 compares kinematic pile-head bending moments between numerical analysis with KIN-SP and the proposed procedure accounting for pile non-linear behavior. Each plot corresponds to a different steel reinforcement ratio while all plots refer to the NC clay profile, in which case the larger bending demand was imposed on the pile. The good agreement between the two solutions showing a deviation of less than 20-25%, provides support on the validity of the proposed procedure beyond the elastic range of both soil and pile response. With reference to piles' filtering action, the $(E_p I_p)_{eff}$ value obtained at the final step of the iteration process may be introduced in Equation 26 to obtain I_u including pile non-linear effects, in the framework of the proposed procedure.

APPLICATION OF SIMPLIFIED FORMULAE IN PILE DESIGN

On the basis of the above results, a practical calculation of kinematic effects on piles may be performed, from a general standpoint, in the following manner:

1. Compute free-field soil response. Since this is the most crucial step, extreme care must be used in the choice of the type of analysis (in case of shear strains above 1% a non linear analysis is strongly recommended) and of the constitutive parameters;

2. Derive mobilized shear modulus. While for an EL analysis this is an automatic output, for non linear analyses this profile may be constructed employing, for any depth, the shear modulus associated, in the G - γ curves, to 0.65 times the maximum shear strain;

3. Perform a linear fit of the shear modulus profile within the pile active length taken as first approximation as 10 pile diameters;

4. Compute pile active length via Equation 14. No further iteration is necessary for linear pile behaviour; If pile nonlinearity is accounted for, compute consecutively: (i) the kinematic moment by Equation 16, (ii) the parameter α and (iii) the effective flexural stiffness $(E_pI_p)_{eff}$ by Equations 29 and 28, respectively, and repeat this step until convergence

5. Compute: (i) γ_{max} at $z_{eff} = L_a / 2$, (ii) the mean frequency of the shear strain time history (Equation 22) and (iii) the frequency reduction factor (Equation 24) to obtain maximum pile kinematic moment by means of Equation 25;

6. Compute pile acceleration time history from Equation 27, by employing Equation 26 for I_u. In the case of a very soft soil at shallow depths like a fully saturated NC Clay, Equation 27 may be still used with confidence, provided that I_u is calculated numerically with the actual distribution of mobilized stiffness instead of the linear fit implied in Equation 26.

CONCLUSIONS

Kinematic pile-head bending moments and foundation input motion were explored under increasing earthquake-induced shear strains in the soil, by means of an advanced 3D Finite Difference model of the soil-pile system, taking into account both stiffness degradation and strength of the soil. Numerical results were compared to the predictions of simple formulae by introducing properly adapted values of the controlling parameters to account for the non-linear soil and pile behavior. The main findings can be summarized as follows:

- While in the linear and static regime the simplified formulae in Equation 16 and 18 return identical predictions of pile-head bending moments, in the non-linear regime of soil response the use of ground surface acceleration is no longer reliable and the maximum shear strain at an effective depth equal to one half of the pile's active length (Equation 15) becomes the dominant soil response parameter controlling kinematic bending at the pile-head.

- The simplified formula in Equation 25 may be employed to derive kinematic pile-head bending in the non-linear dynamic range of soil response. In this regard, a 1D free-field non-linear soil response analysis, which properly considers both stiffness degradation and soil strength, should be performed to derive the necessary parameters employed in the formulae. Consideration of pile non-linear response is also possible in the framework of the proposed procedure by means of an effective stiffness of the pile's section (Equation 28) derived on the basis of a relevant moment – curvature relation.
- Following up on the above comments, a mean cyclic frequency was suggested (Equation 23) as a single index of the frequency content of the shear strain time history at one half of the pile's active length, following the definition of the mean period introduced in Rathje et al. 1998 for an acceleration time history. Such an interpretation of the frequency content of a shear strain time history has not been previously explored in the kinematic response of piles.
- A linear fit is proposed as a simple model of the mobilized shear stiffness profile from free-field soil response analysis, which holds in both linear and non-linear regime of soil response.
- Similarly, the assessment of piles' filtering effects on the seismic loading imposed at the superstructure is possible, even at large strain levels, via the combination of the results of proper soil response analysis and the simple formula in Equation 26. In the case of a fully saturated NC Clay, a numerically-derived I_u based on the actual distribution of the mobilized stiffness is suggested instead of the linear fit.
- The structural period corresponding to the maximum pile-induced filtering of the free-field motion at ground surface is independent of the input motion properties even if the soil undergoes large shear strains.

- It was proven that dynamic and non-linear effects result in modifying solely soil deformations at free-field conditions, while soil-pile kinematic interaction mechanism remains static and (equivalent) linear, which means that the dynamic nature of kinematic pile response stems from the superposition of a dynamic phenomenon, referring to ground response under earthquake shaking and a static problem related to pile-soil interaction. This shed lights to the actual nature of kinematic soil-pile interaction, denoting that the associated mechanism is stiffness-controlled even if free-field soil response is strength-controlled.
- A work-flow for a practical calculation of kinematic effects accounting for both soil and pile non-linear response is provided that facilitates their consideration in the seismic design of piles.

It is fair to mention that some of the conclusions reported above may require revision in case of soils susceptible to liquefaction or more generally when shear-induced pore water pressures are of major concern (i.e., those cases in which an advanced effective stress analysis of seismic response is necessary).

DATA AVAILABILITY STATEMENT

Data regarding FLAC, ANSYS, and DEEPSOIL analyses are available from the corresponding author upon reasonable request.

ACKNOWLEDGEMENTS

The authors wish to thank ITASCA for a loan of software within the Itasca Education Partnership (IEP). The corresponding author wish to thank Universita della Campania Luigi Vanvitelli for partially funding this work, through Programma V:ALERE 2020, project ‘Piles AS SEismic vulnerability Reduction Appliances’.

REFERENCES

Afacan, K. B., Brandenberg, S. J. and Stewart, J. P. 2013. Centrifuge modeling studies of site response in soft clay over wide strain range, Journal of Geotechnical and Geoenvironmental Engineering, 140(2): 04013003.

Ancheta, T., Darragh, R., Stewart, J.P., Seyhan, E., Silva, W., Chiou, B., Wooddell, K., Graves, R., Kottke, A., Boore, D., Kishida, T., and Donahue, J. 2013. PEER NGA-West2 Database, PEER Report 2013/03 Pacific Earthquake Engineering Research Center Headquarters at the University of California, Berkeley.

Anoyatis, G., Di Laora, R., Mandolini, A., and Mylonakis, G. 2013. Kinematic response of single piles for different boundary conditions: Analytical solutions and normalization scheme. Soil Dynamics and Earthquake Engineering, 44: 183-195.

ANSYS 15.0, software. Canonsburg, PA, ANSYS.

Comité Euro-International du Béton. CEB-FIP Model Code 1990; Bulletin d'Information: Telford, UK, 1993.

CEN. EN 1998-4: Design of structures for earthquake resistance, Part 1: General rules, seismic actions and rules for buildings, Brussels: European Committee for Standardization; 2004.

Conti, R., Di Laora R., Licata V., Iovino M. and de Sanctis L. 2020. Seismic performance of bridge piers: caisson vs pile foundations. Soil Dynamics and Earthquake Engineering. 130, 105985.

de Sanctis, L., Maiorano, R.M.S. and Aversa, S. 2010. A method for assessing kinematic bending moments at the pile head. Earthquake Engineering and Structural Dynamics, 39(4), 1133-1154.

Di Laora, R. and de Sanctis, L. 2013. Piles-induced filtering effect on the Foundation Input Motion. Soil Dynamics and Earthquake Engineering. 46: 52-63.

Di Laora, R. and Rovithis, E. 2015. Kinematic bending of fixed-head piles in nonhomogeneous soil. Journal of the Geotechnical Engineering Division, 141(4): 04014126.

Di Laora, R., Mandolini, A. and Mylonakis, G. 2012. Insight on kinematic bending of flexible piles in layered soil. Soil Dynamics and Earthquake Engineering, 43: 309-322.

Di Laora, R., Mylonakis, G. and Mandolini, A. 2017. Size limitations for piles in seismic regions. Earthquake Spectra, 33(2): 729-756.

Di Laora R. and Rovithis E. 2021. Design of piles under seismic loading, In Pile Foundations Under Static and Dynamic Loads (A. Kaynia ed), ISBN 9780367374167, DOI: 10.1201/9780429354281-8.

Dobry, R. and O'Rourke, M.J. 1983. Discussion on 'Seismic response of end-bearing piles' by Flores-Berrones R and Whitman R.V. Journal of the Geotechnical Engineering Division, 109(5), 778.

Dezi, F., Carbonari, S., and Leoni, G. 2010. Kinematic bending moments in pile foundations. Soil Dynamics and Earthquake Engineering, 30(3), 119-132.

Elgamal, A., Yan, L., Yang Z., and Conte., J. P. 2008. Three-dimensional seismic response of Humboldt Bay bridge foundation-ground System, Journal of Structural Engineering, ASCE, 134(7): 1165-1176.

Flores-Berrones, R., and Whitman, R. V. 1982. Seismic response of end bearing piles. Journal of the Geotechnical Engineering Division ASCE, 108(4): 554-569.

Garala, T. K. and Madabhushi, G. S. P. 2019. Seismic behaviour of soft clay and its influence on the response of friction pile foundations, Bulletin of Earthquake Engineering, 17: 1919–1939.

Garala, T. K., Madabhushi, G. S. P. and Di Laora R. 2020. Experimental investigation of kinematic pile bending in layered soils using dynamic centrifuge modeling. Geotechnique, https://doi.org/10.1680/jgeot.19.P.185

Gazetas, G. 1984. Seismic response of end-bearing single piles. Soil Dynamics and Earthquake Engineering, 3(2): 82-93.

Groholski, D.R., Hashash, Y.M.A., Kim, B., Musgrove, M., Harmon, J. and Stewart, J.P. 2016. Simplified model for small-strain nonlinearity and strength in 1D seismic response analysis. Journal of Geotechnical and Geoenviromental Engineering, 142(9): 04016042.

Groholski, D.R., Hashash, Y.M.A., Musgrove, M., Harmon, J. and Kim, B. 2015. Evaluation of 1-D Non-linear site response analysis using a general quadratic/hyperbolic strength-controlled constitutive model. Proceedings of the 6th International Conference on Earthquake Geotechnical Engineering, Christchurch, New Zealand.

Hardin, B.O. and Richart, E. F. Jr. 1963. Elastic Wave Velocities in Granular Soils. Journal of the Soil Mechanics and Foundation Division, ASCE, 89(SM1): 33–65.

Hashash, Y. M. A., Phillips, C. and Groholski, D.R. 2010. Recent Advances in non-linear soil response analysis. Proceedings of the 5th International Conference on Recent Advances in Geotechnical Earthquake Engineering and Soil Dynamics, San Diego, California.

Hashash, Y.M.A., Musgrove, M.I., Harmon, J.A., Groholski, D.R., Philips, C.A. and Park, D. 2016. DEEPSOIL 6.1 User Manual, 2016.

Iovino M., Di Laora R., Rovithis Emm. and de Sanctis L. 2019. The beneficial role of piles on the seismic loading of structures, Earthquake Spectra, 35(3):1141-1162.

Itasca 2017. Fast Lagrangian Analysis of Continua (FLAC3D 6.00). Itasca Consulting Group Inc, Minneapolis, USA (2017)

Kaklamanos, J., Bradley, B. A., Thompson, E. M. and Baise, L. G. 2013. Critical parameters affecting bias and variability in site-response analyses using KiK-net downhole array data. Bulletin of the Seismological Society of America, 103(3): 1733-1749.

Karatzia, X. and Mylonakis, G., 2016. Discussion of kinematic bending of fixed-head piles in nonhomogeneous soil by Raffaele Di Laora and Emmanouil Rovithis, Journal of Geotechnical and Geoenvironmental Engineering, 142(2): 07015042.

Kawamura, S., Umemura, S. H., Osawa, Y. 1977. Earthquake motion measurement of a pile supported building on reclaimed ground. Proceedings of the 6th World Conference on Earthquake Engineering, India.

Kaynia, A. M., and Kausel, E., 1991. Dynamics of piles and pile groups in layered soil media. Soil Dynamics and Earthquake Engineering 10(8): 386-401.

Kuhlemeyer, R.L. and Lysmer. J. 1973. Finite element method accuracy for wave propagation problems. Journal of the Soil Dynamics Division, 99: 421-427.

Kwok, A., Stewart, J. P., Hashash, Y. M. A., Matasovic, N., Pyke, R., Wang, Z., and Yang, Z. 2007. Use of exact solutions of wave propagation problems to guide implementation of nonlinear seismic ground response analysis procedures. Journal of Geotechnical and Geoenvironmental Engineering, 133: 1385-1398.

Ladd, C. C., Foott, R., Ishihara, K., Schlosser, F., and Poulos, H. G. 1977. Stress-deformation and strength characteristics. Proceedings of the 9th International Conference on Soil Mechanics and Foundation Engineering, Tokyo, Vol. 2: 421-494.

Licata, V., Conti, R., Di Laora, R., de Sanctis, L., Mittiga, E. and Micheli, A. 2019. Seismic design of deep pier foundations in very soft clayey soils. Proceedings of the 7th lnternational Conference on Earthquake Geotechnical Engineering, Rome, 17-20 June 2019.

Maiorano, R.M.S., de Sanctis, L., Aversa, S. and Mandolini, A. 2009. Kinematic response analysis of piled foundations under seismic excitations. Canadian Geotechnical Journal, 46(5), 571-584.

Mamoon, S. M., and Banerjee, P. K., 1990. Response of piles and pile groups to traveling SH-waves, Earthquake Engineering & Structural Dynamics 19(4): 597-610.

Mander, J.B.; Priestley, M.J.; Park, R. 1988. Theoretical stress-strain model for confined concrete. Journal of Structural Engineering, 114: 1804–1826.

Matasovic, N. 1993. Seismic response of composite horizontally-layered soil deposits. Ph.D. Thesis, University of California, Los Angeles.

Meyerhof, G.G. 1957. Discussion on Research on determining the density of sands by penetration testing. Proceedings of the 4th International Conference on Soil Mechanics and Foundation Engineering, Vol. 1: 110

Mizuno, H. 1987. Pile Damage during Earthquake in Japan. In: Nogami T, editor. Dynamic Response of Pile Foundations, ASCE Special Publication.

Mucciacciaro, M., and Sica, S. 2018. Nonlinear soil and pile behaviour on kinematic bending response of flexible piles. Soil Dynamics and Earthquake Engineering, 107: 195-213.

Mylonakis, G. 2001. Simplified model for seismic pile bending at soil layer interfaces. Soils and Foundations, 41(4), 47-58.

Nikolaou, A., Mylonakis, G., Gazetas, G. and Tazoh, T. 2001. Kinematic pile bending during earthquakes: Analysis and field measurements. Geotechnique, 51(5): 425-440.

Ohta, T., Uchiyama, S., Niwa, M., Ueno, K. 1980. Earthquake response characteristics of structure with pile foundation on soft subsoil layer and its simulation analysis. Proceedings of the 7th World Conference on Earthquake Engineering, Vol. 3. Istanbul, Turkey.

Phillips, C. and Hashash, Y.M.A. 2009. Damping formulation for non-linear 1D site response analyses. Soil Dynamics and Earthquake Engineering, 29: 1143-1158.

Popovics, S 1973. A numerical approach to the complete stress-strain curve of concrete. Cement and Concrete Research, 3: 583–599.

Rathje, E.M., Abrahamson, N.A and Bray, J.D. 1998. Simplified frequency contents estimates of earthquake ground motions. Journal of Geotechnical and Geoenviromental Engineering, 124(2): 150-158.

Rovithis, E., Parashakis, Ch. and Mylonakis, G. 2011. 1D harmonic response of layered inhomogeneous soil: Analytical investigation, Soil Dynamics and Earthquake Engineering, 31: 879-890.

Rovithis, E., Mylonakis, G., and Pitilakis, K., 2013. Dynamic stiffness and kinematic response of piles in inhomogeneous soil. Bulletin of Earthquake Engineering 11(6): 1949-1972.

Seed, H. B. and Idriss, I. M. 1970. Soil Moduli and Damping Factors for Dynamic Response Analyses. Report EERC 70-10, Earthquake Engineering Research Center, University of California, Berkeley.

Sica, S., Mylonakis, G. and Simonelli, A.L. 2011. Transient kinematic pile bending in two-layer soil. Soil Dynamics and Earthquake Engineering, 31(7), 891-905.

Shi, J. And Asimaki D. 2017. From stiffness to strength: Formulation and validation of a hybrid hyperbolic nonlinear soil model for site-response analyses. Bulletin of the Seismological Society of America, 107(3): 1336-1355.

Skempton, A. W. 1957. Discussion: Further data on the c/p ratio in normally consolidated clays. Proceedings of the Institution of Civil Engineers 7, 305–307.

Stacul, S., & Squeglia, N. 2018. KIN SP: A boundary element method based code for single pile kinematic bending in layered soil. Journal of Rock Mechanics and Geotechnical Engineering, 10(1): 176-187.

Stacul, S. and Squeglia N. 2020. Simplified assessment of pile-head kinematic demand in layered soil. Soil Dynamics and Earthquake Engineering, 130: 105975.

Tazoh, T., Shimizu, K. and Wakahara, T. 1987. Seismic observations and analysis of grouped piles. In Dynamic response of pile foundations: experiments, analysis and observation, Geotechnical Special Publication No.11, ASCE, 1987.

Travasarou, T. and Gazetas, G. 2004. On the linear seismic response of soils with modulus varying as a power of depth – The Maliakos marine clay. Soils and Foundations, 44: 85-93.

Vardanega, P.J. and Bolton M. D. 2013. Stiffness of clays and silts: Normalizing shear modulus and shear strain. Journal of Geotechnical and Geoenviromental Engineering, 139(9): 1575-1589.

Vucetic, M. and Dobry, R. 1991. Effect of soil plasticity on cyclic response. Journal of Geotechnical Engineering, 17: 89-107.

Weiler, W. A. 1988. Small-strain shear modulus of clay. Proceedings of the Specialty Conference on Earthquake Engineering and Soil Dynamics II - Recent Advances in Ground-Motion evaluation, Geotechnical Special Publication No. 20, ASCE, 1988, pp. 331-345.

Zhou, Y.G., Chen, J., Chen, Y., Kutter, B. L., Zheng, B., Wilson, D. W., Stringer, M. E., and Clukey, E. C. 2017. Centrifuge modelling and numerical analysis on seismic site response of deep offshore clay deposits. Engineering Geology, 227: 54–68.

TABLES

Table 1: Earthquake metadata of the seven input motions, as reported in the PEER Strong Motion Database (Ancheta et al. 2013)

Motion name	Record number	Date	Magnitude	Distance to fault rupture (km)	PGA (g)	EC8 soil type
WhittierNarrows	P0666	01/10/1987	6	21.2	0.186	A
Coyote	P0154	06/08/1979	5.7	17.2	0.124	A
Kocaeli	P1087	17/08/1999	7.4	17	0.218	A
LomaGilroy	P0738	18/10/1989	6.9	19.9	0.170	A
Mammothlake	P0232	25/05/1980	6.3	15.5	0.430	A
Nahanni	P0498	23/12/1985	6.8	16	0.148	A
Northridge	P1014	17/10/1994	6.7	26.8	0.217	A

Table 2: Physical and mechanical parameters of the soil profile in the Po Valley (Conti et al. 2020)

Soil type	Depth z (m)	Thickness (m)	V_s (m/s)	γ (kN/m^3)	c_u (kPa)	φ (°)
MG	0-5	5	125	18	40	23
CS	5-14	9	130	16	50	20
P	14-16	2	97	12	32	28
CS	16-20	4	170	16	120	20
	20-24	4	200	16	120	20
SS	24-29	5	235	18	-	30
CS	29-40	11	250	18	180	22
	40-60	20	350	18	290	22
	60-80	20	450	18	400	22
	80-100	20	500	18	520	22

Table 3: Pile section properties varying the steel reinforcement ratio (*d* = 1m)

	A_s / A_c (%)			
	0.5	1	2	4
$(E_pI_p)_{uncracked}$ $[MNm^2]$	1227	1227	1227	1227
M_{cr} $[kNm]$	379	405	448	539
$(E_pI_p)_{cracked}$ $[MNm^2]$	57	235	489	946
M_y $[kNm]$	533	1074	1892	3584
M_{ult} $[kNm]$	777	1556	2771	5088
$(E_pI_p)_{uncracked}$ $[MNm^2]$	1227	1227	1227	1227

Table 4: Pile section properties varying the steel reinforcement ratio (d = 1.5 m)

	A_s / A_c (%)			
	0.5	1	2	4
$(E_pI_p)_{uncracked}$ $[MNm^2]$	6213	6213	6213	6213
M_{cr} $[kNm]$	1294	1367	1534	1858
$(E_pI_p)_{cracked}$ $[MNm^2]$	335	1083	2456	4855
M_y $[kNm]$	1873	3475	6936	12229
M_{ult} $[kNm]$	2793	4922	9441	17387
$(E_pI_p)_{uncracked}$ $[MNm^2]$	6213	6213	6213	6213

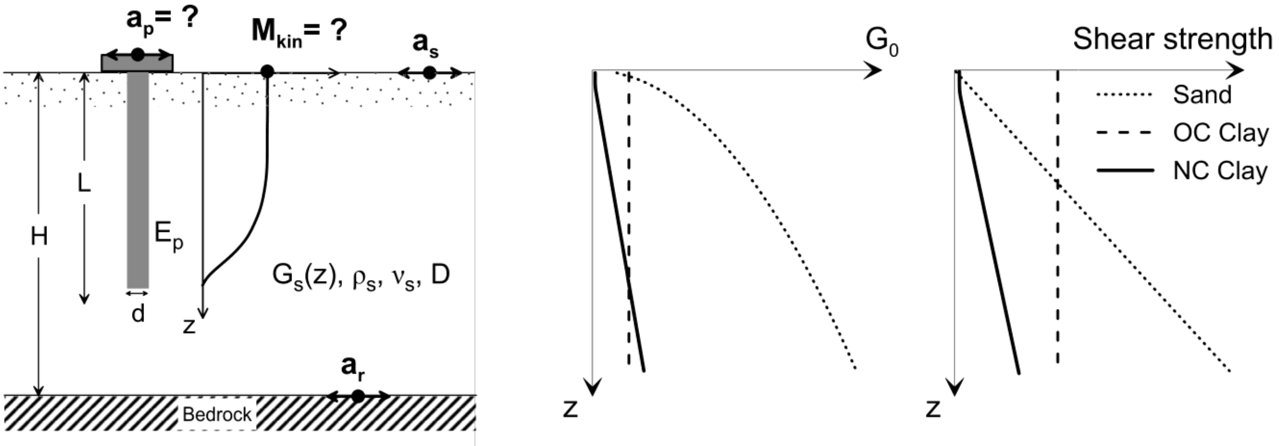

Figure 1: Single elastic fixed-head pile embedded in three soil profiles under examination

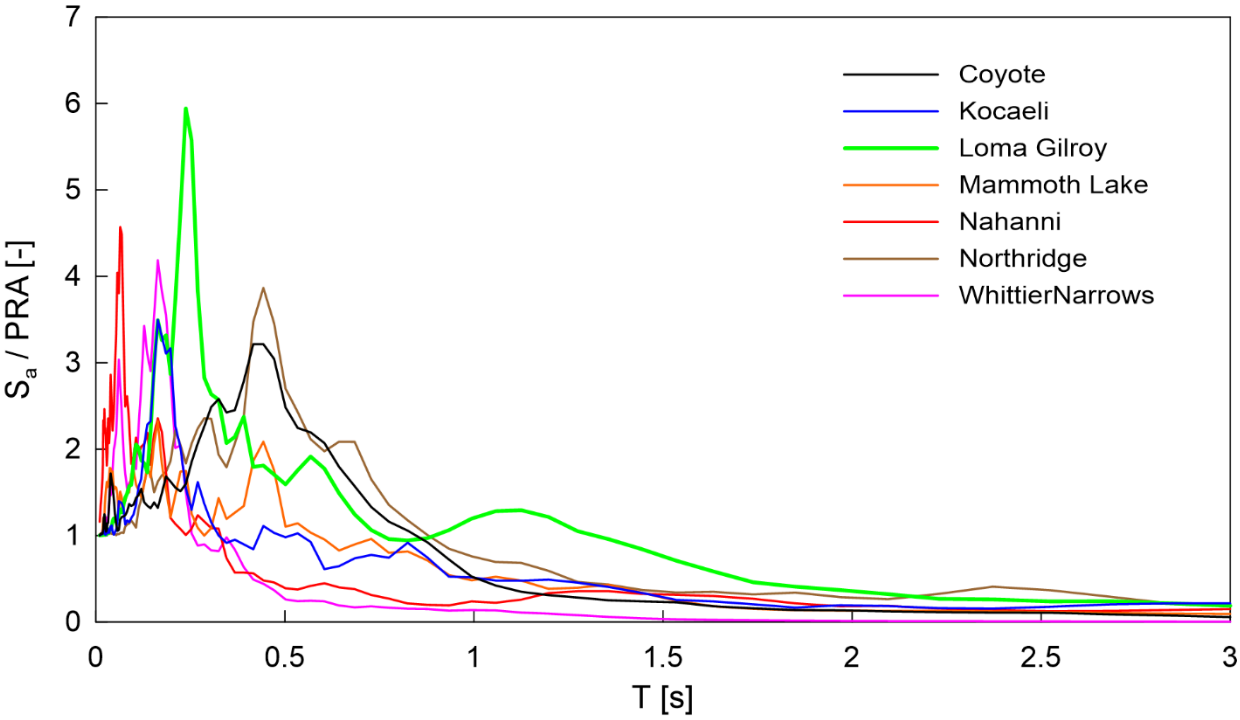

Figure 2: Normalized elastic response acceleratiton spectra of the selected input motions

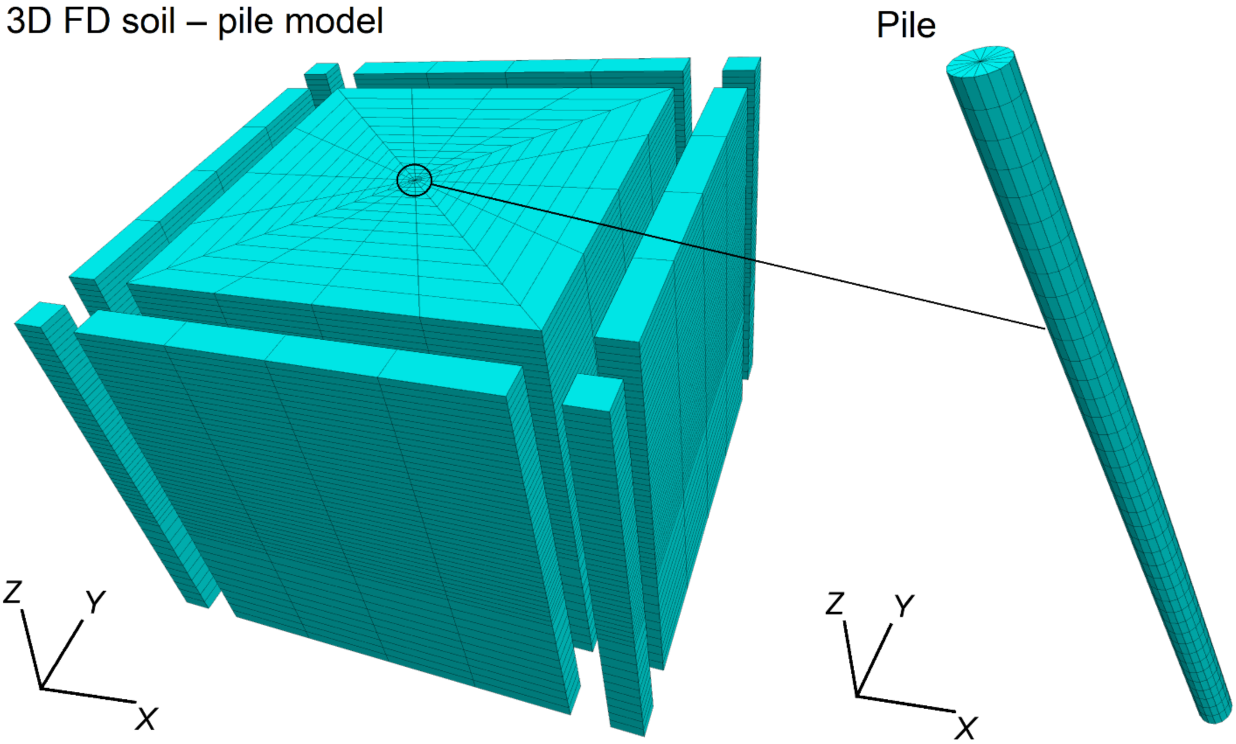

Figure 3: FLAC3D numerical model.

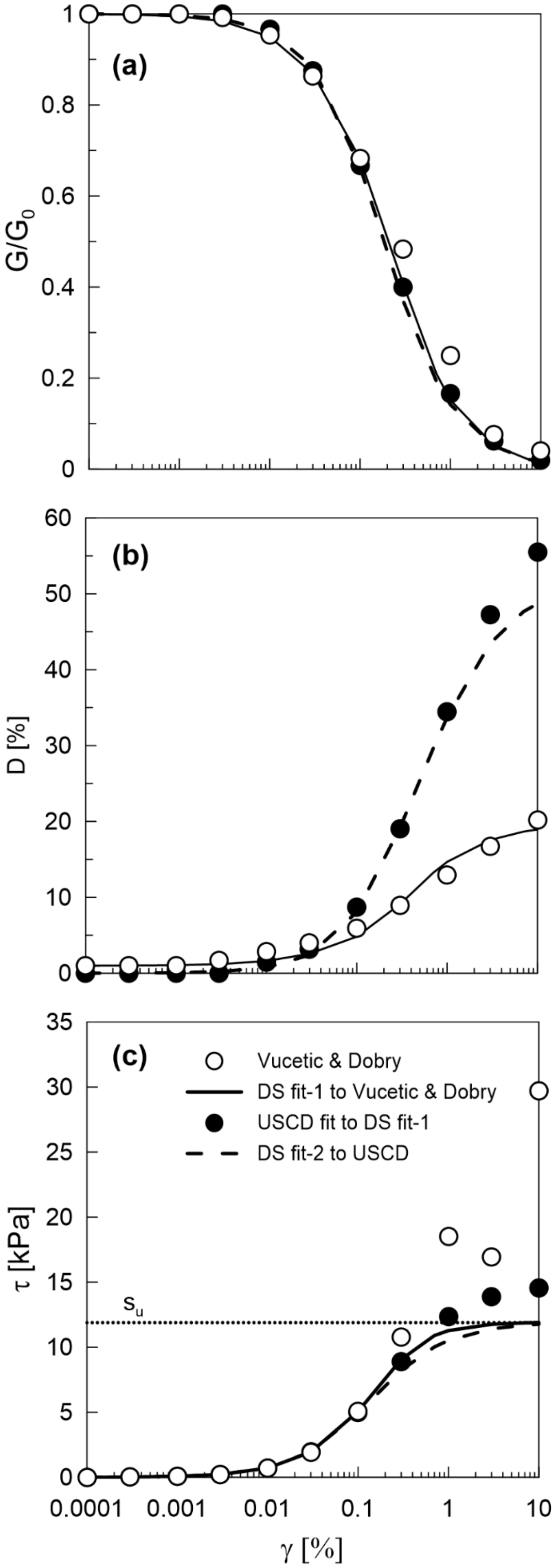

Figure 4: Calibration of DEEPSOIL and FLAC3D soil models for the NC Clay case based on Vucetic and Dobry (1991) $G/G_0 - \gamma - D(\%)$ curves for $I_p = 40\%$ regarding: (a) Stiffness degradation, (b) Hysteretic damping increase and (c) Shear stress-strain backbone curve at the depth of 4.375m (the implied shear strength derived in DEEPSOIL is also mentioned)

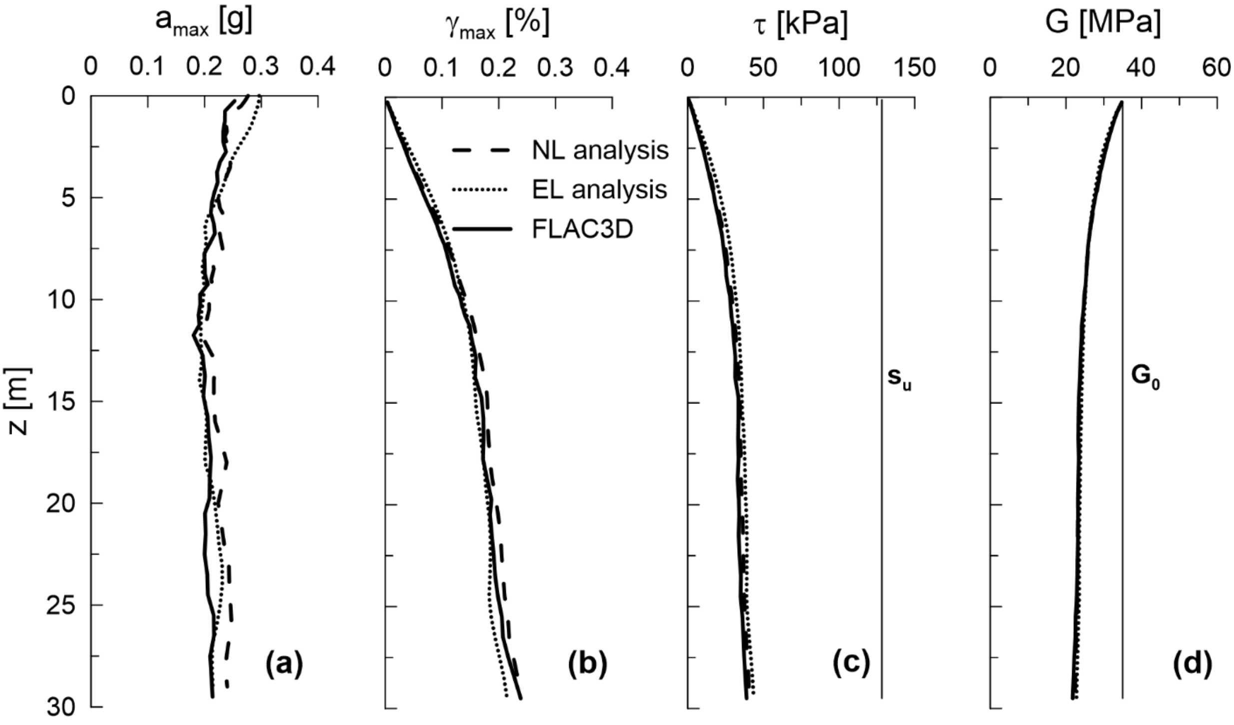

Figure 5: Comparison of free-field ground response analysis results between DEEPSOIL (EL and NL analysis) and FLAC3D for the OC clay profile in terms of: (a) average PGA profile (b) average maximum shear strain profile (c) average shear stress and (d) average mobilized shear modulus *G* with depth. All plots refer to PRA = 0.25g.

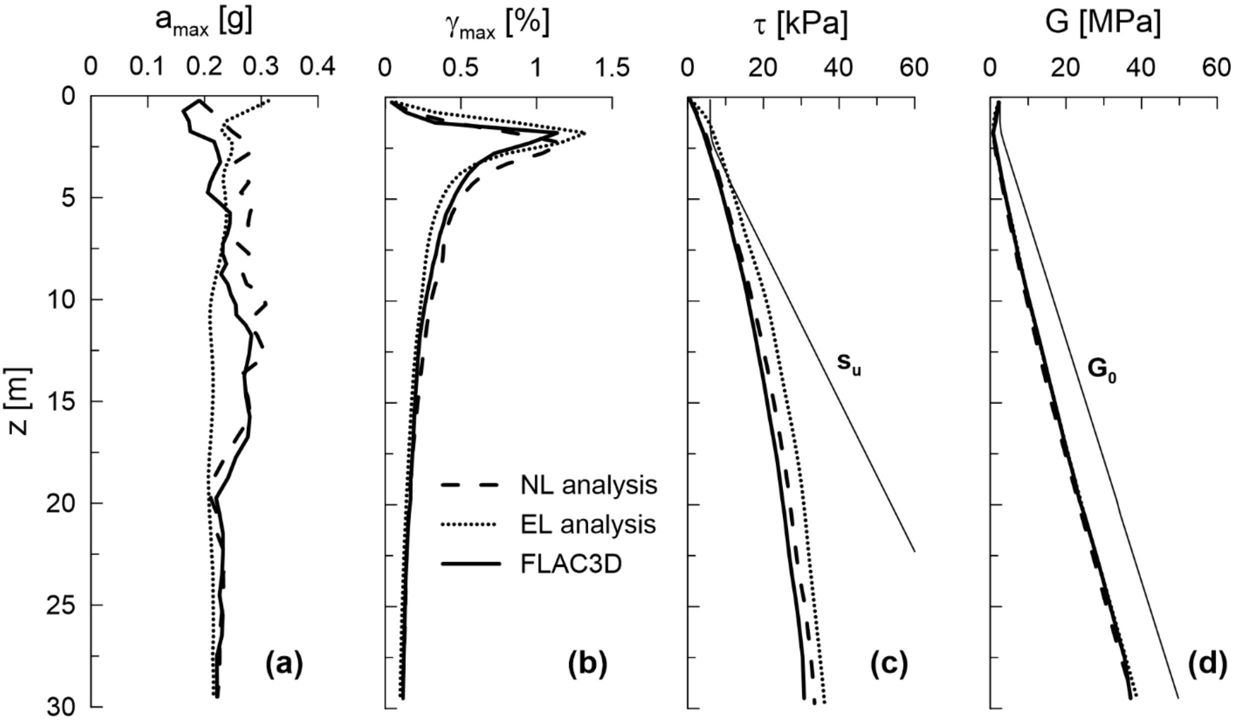

Figure 6: Comparison of free-field ground response analysis results between DEEPSOIL (EL and NL analysis) and FLAC3D for the NC clay profile in terms of: (a) average PGA profile (b) average maximum shear strain profile (c) average shear stress and (d) mobilized shear modulus *G* with depth. All plots refer to PRA = 0.25g.

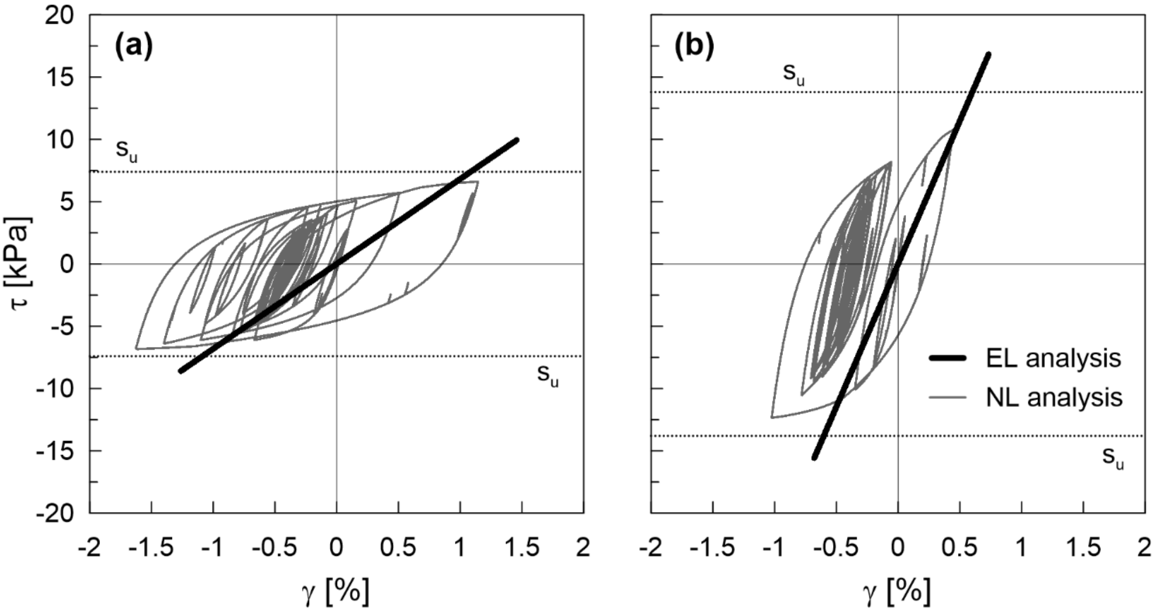

Figure 7: Comparison of EL and NL soil response analysis with DEEPSOIL for the NC clay profile in terms of τ - γ loops at the depth of: (a) 2.625 m and (b) 5.125 m. All plots refer to PRA = 0.25g.

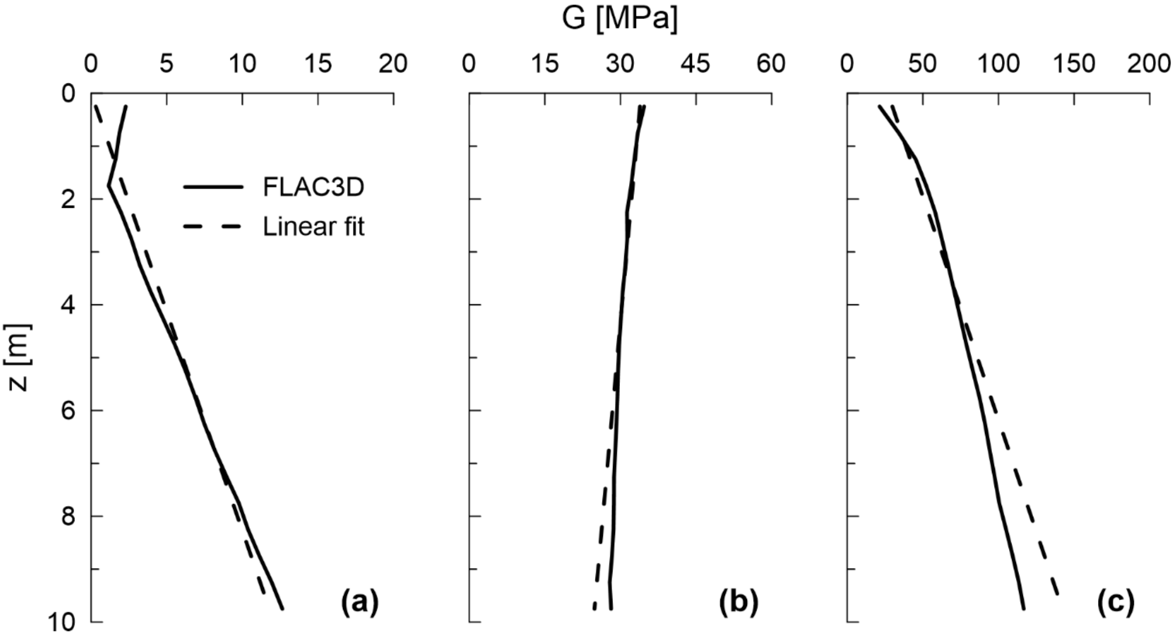

Figure 8: Linear fit of the mobilized shear modulus profile obtained with FLAC3D at free-field conditions under the Nahanni record scaled to PRA = 0.25g for the (a) NC Clay (b) OC Clay and (c) Sand profile

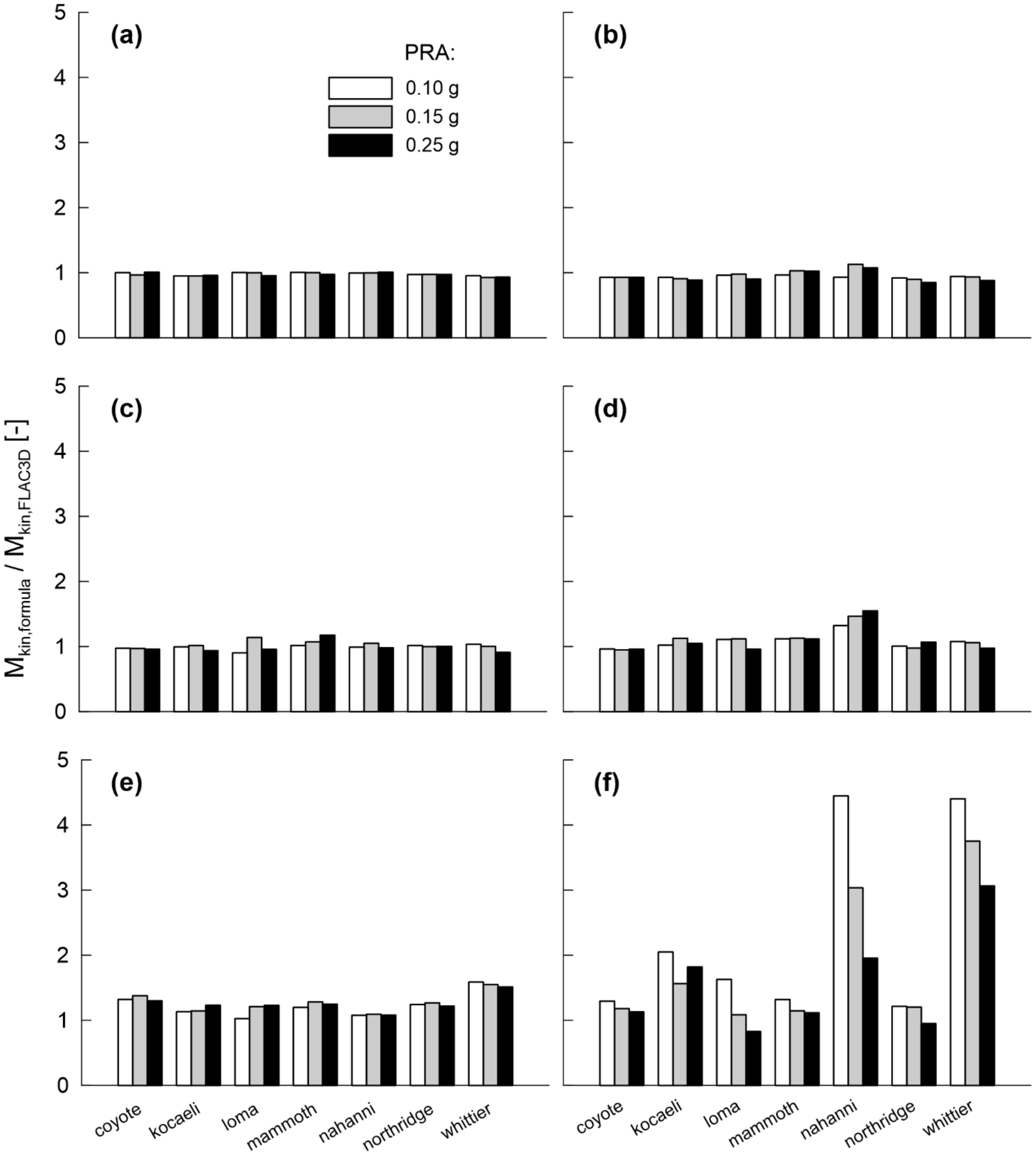

Figure 9: Ratios of kinematic pile-head bending moment between the predictions of Equation 16 (left graphs) and Equation 18 (right graphs) and 3D FD analyses (FLAC3D): (a, b) Sand profile (c, d) OC Clay profile and (e, f) NC Clay profile.

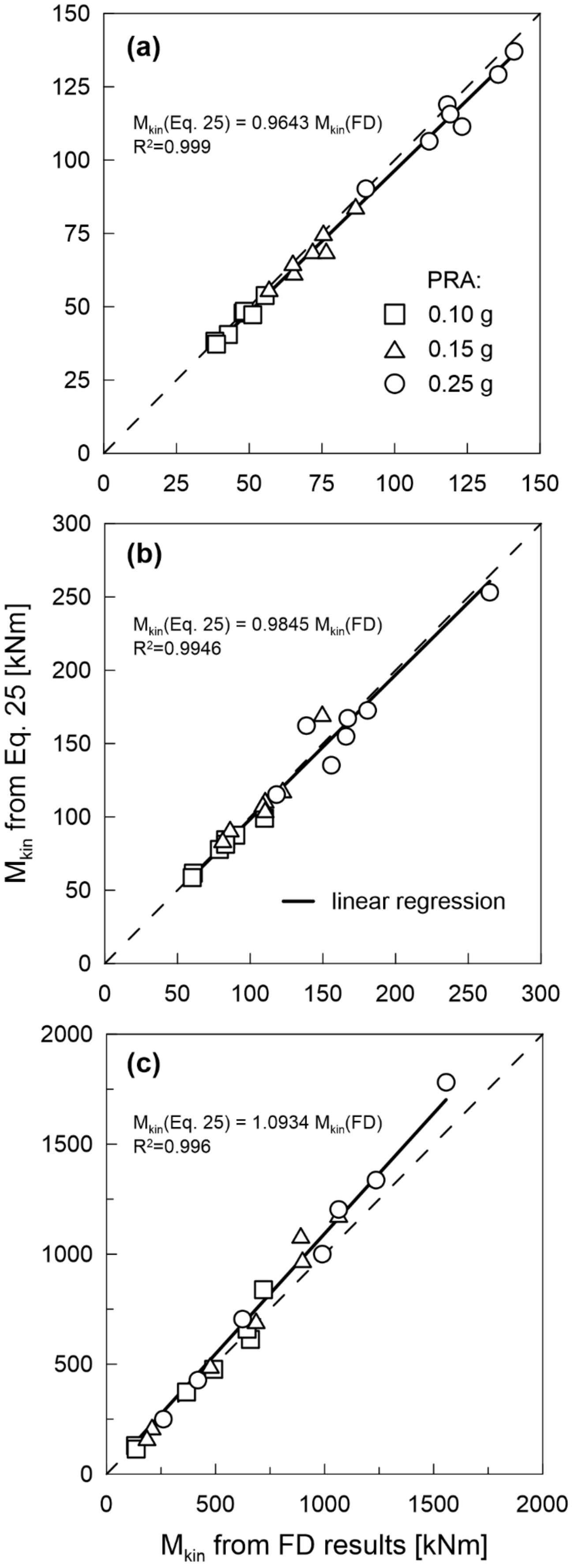

Figure 10: Comparison of kinematic pile-head bending moments between Equation 25 and FD results for the (a) Sand (b) OC Clay and (c) NC Clay profiles. Each point in the plots refers to a different input motion.

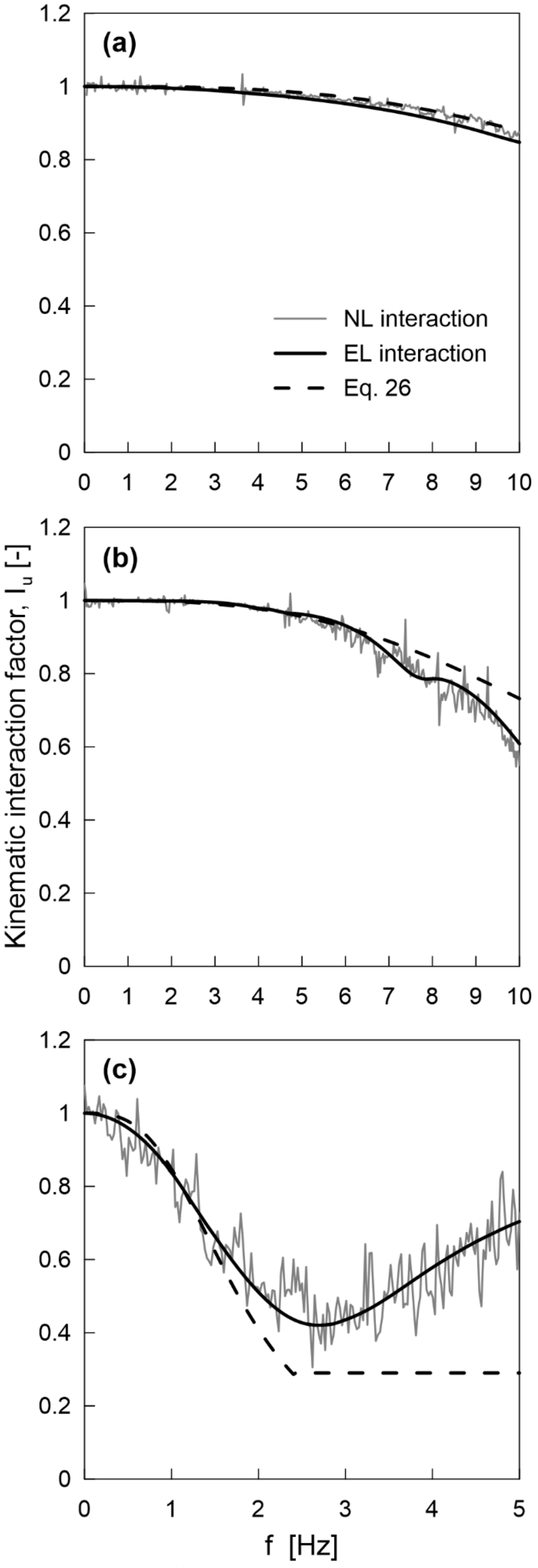

Figure 11: Amplitude of average kinematic interaction factor *I_u* derived by different modeling assumptions for (a) Sand (b) OC Clay and (c) NC Clay soil. All plots refer to PRA = 0.10g.

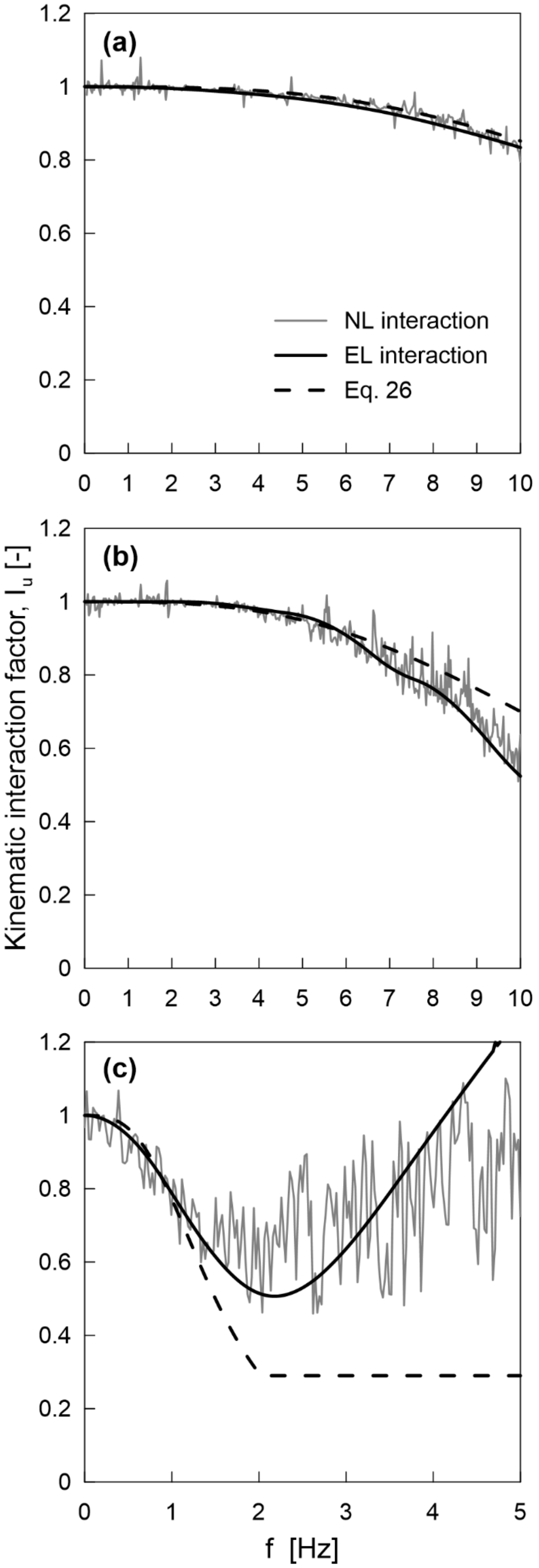

Figure 12: Amplitude of average kinematic interaction factor I_u derived by different modeling assumptions for (a) Sand (b) OC Clay and (c) NC Clay soil. All plots refer to PRA = 0.25g.

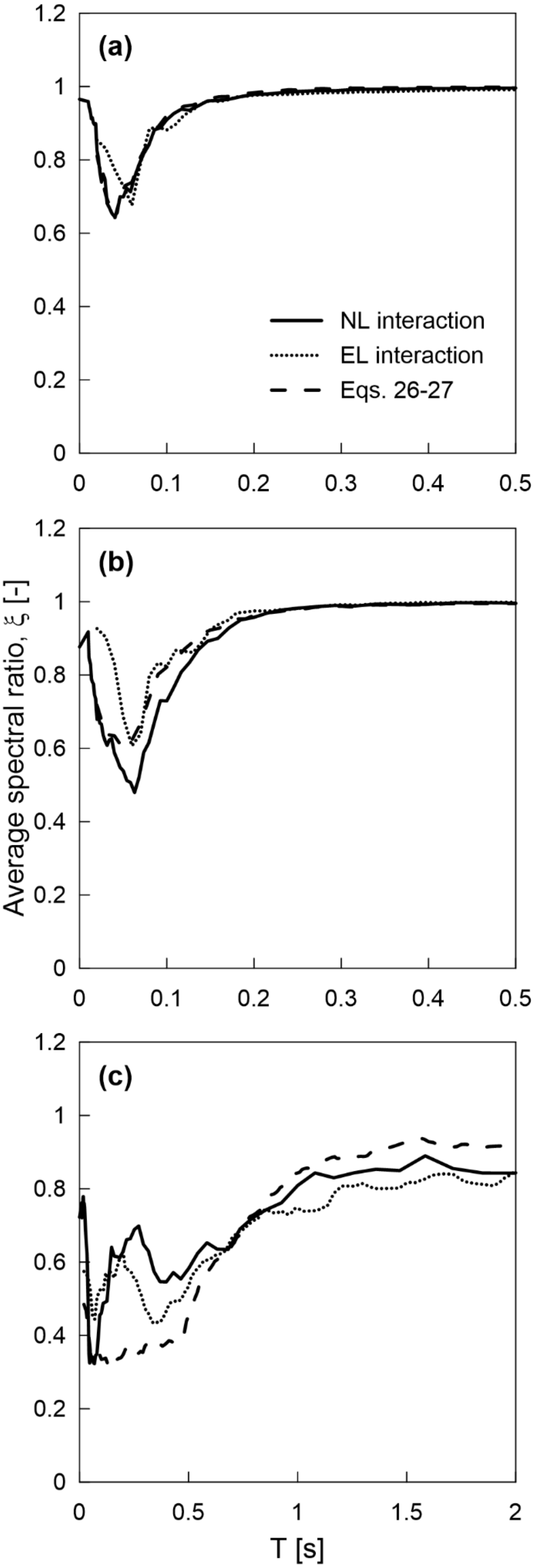

Figure 13: Comparison of average spectral ratios obtained with FLAC3D, ANSYS (FLAC3D-based stiffness) and Iovino et al. (2019) simplified procedure for (a) Sand, (b) OC Clay and (c) NC Clay soil. Plots refer to PRA = 0.10g.

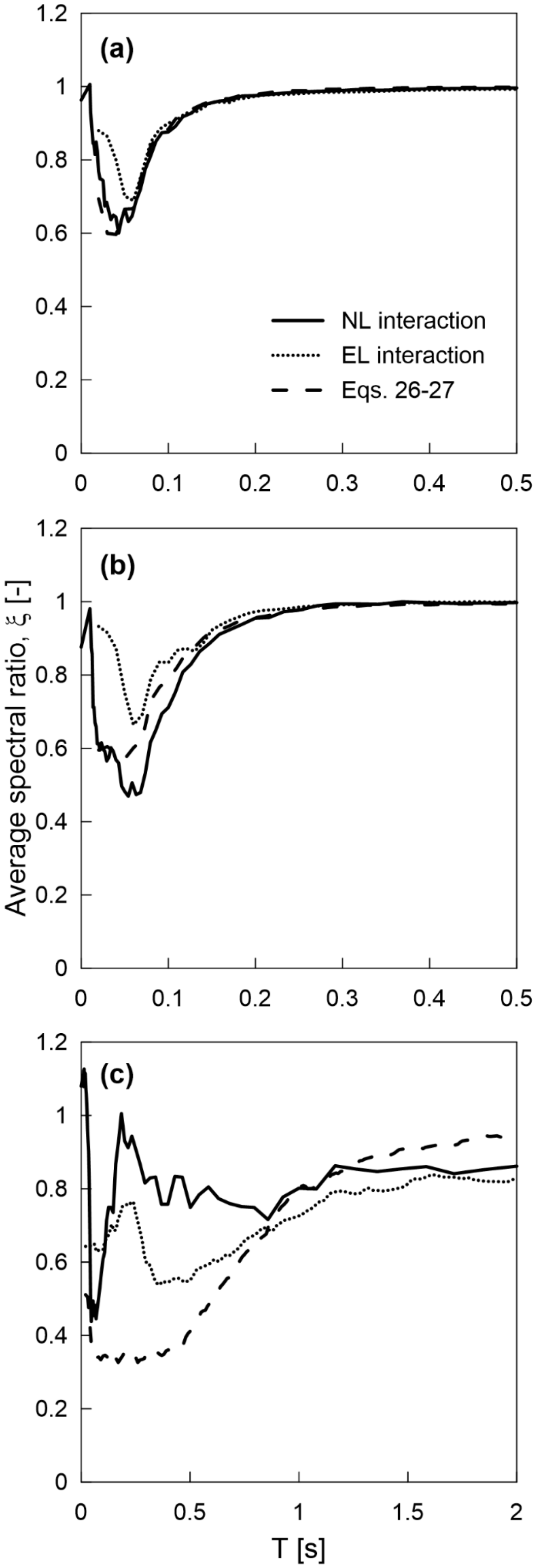

Figure 14: Comparison of average spectral ratios obtained with FLAC3D, ANSYS (FLAC3D-based stiffness) and Iovino et al. (2019) simplified procedure for (a) Sand, (b) OC Clay and (c) NC Clay soil. Plots refer to PRA = 0.25g.

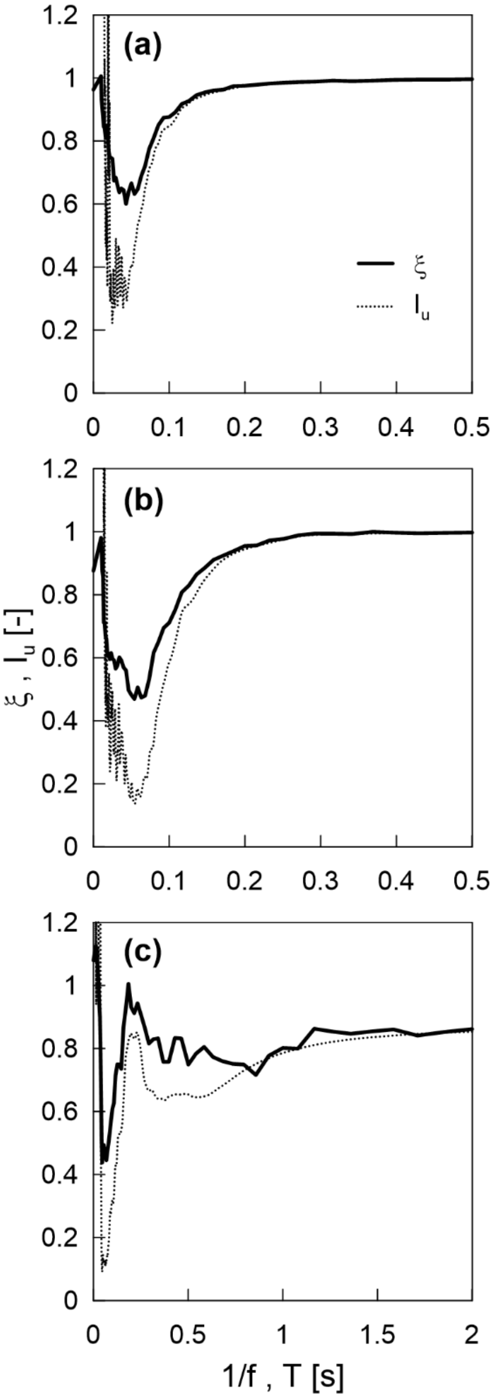

Figure 15: Comparison of average kinematic interaction factor as function of 1⁄f and average spectral ratios as function of structural period for (a) Sand, (b) OC Clay and (c) NC Clay soil. All plots refer to FLAC3D results obtained for PRA = 0.25g.

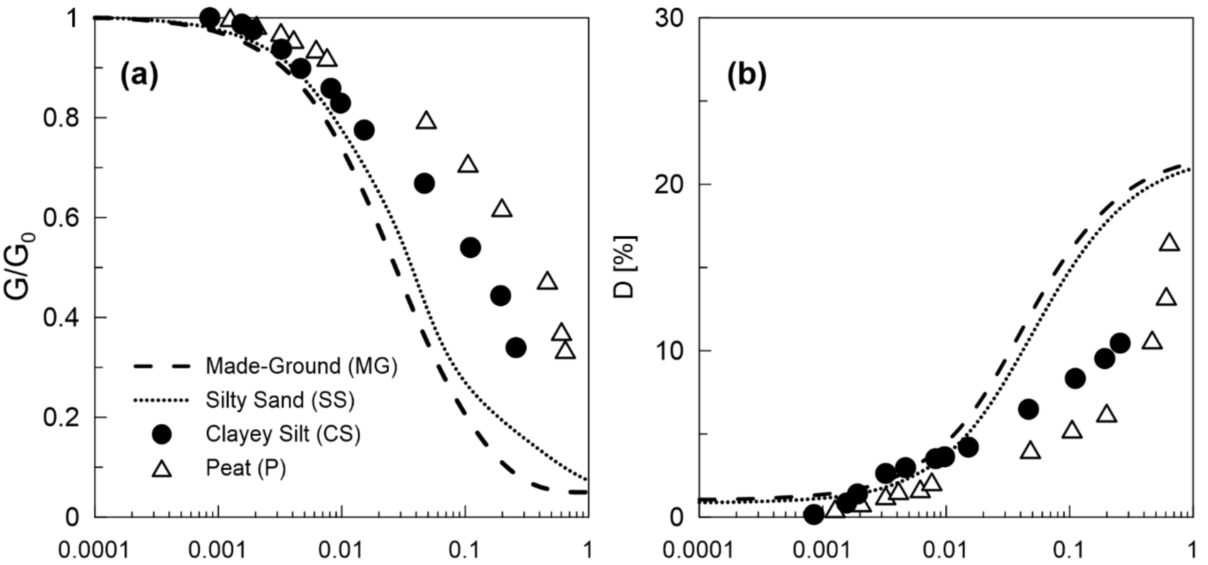

Figure 16: Shear modulus degradation (a) and hysteretic damping (b) curves for the soil types in the layered profile under consideration (modified after Conti et al. 2020)

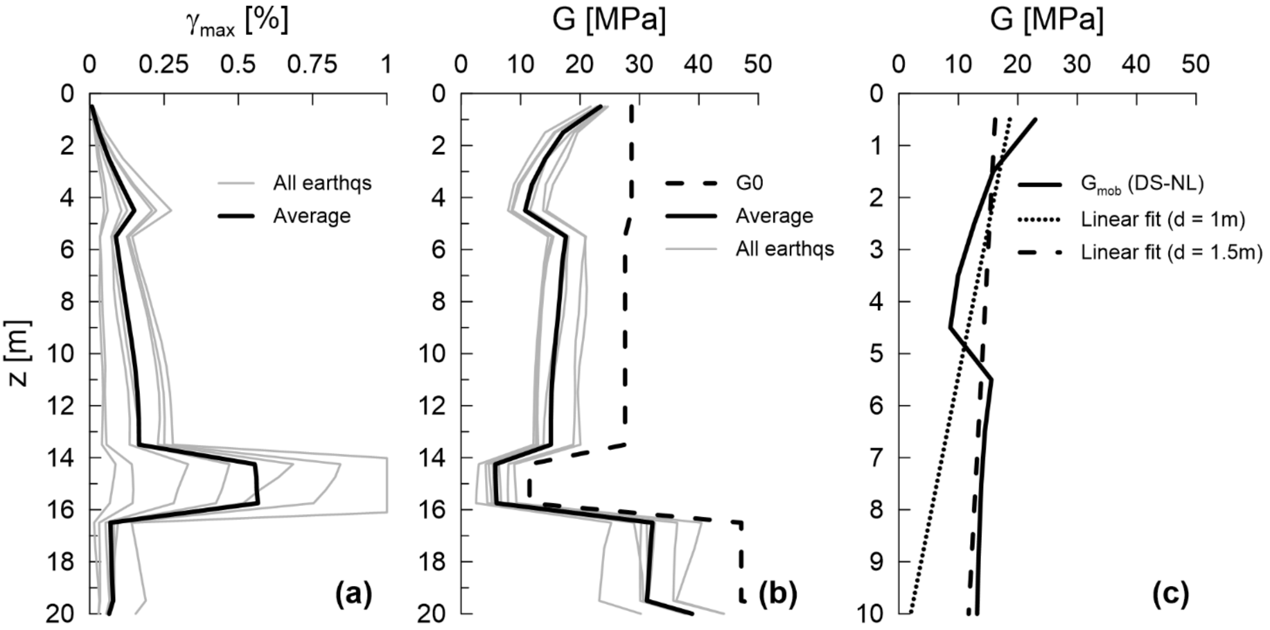

Figure 17: Ground response results obtained from Deepsoil NL analysis of the layered profile in the Po Valley area: (a) mobilized shear modulus *G* profile with depth (b) maximum strain profile with depth and (c) linear fit of the mobilized shear modulus profile under the Coyote input motion for each one of the considered pile diameters. All plots refer to PRA = 0.15g.

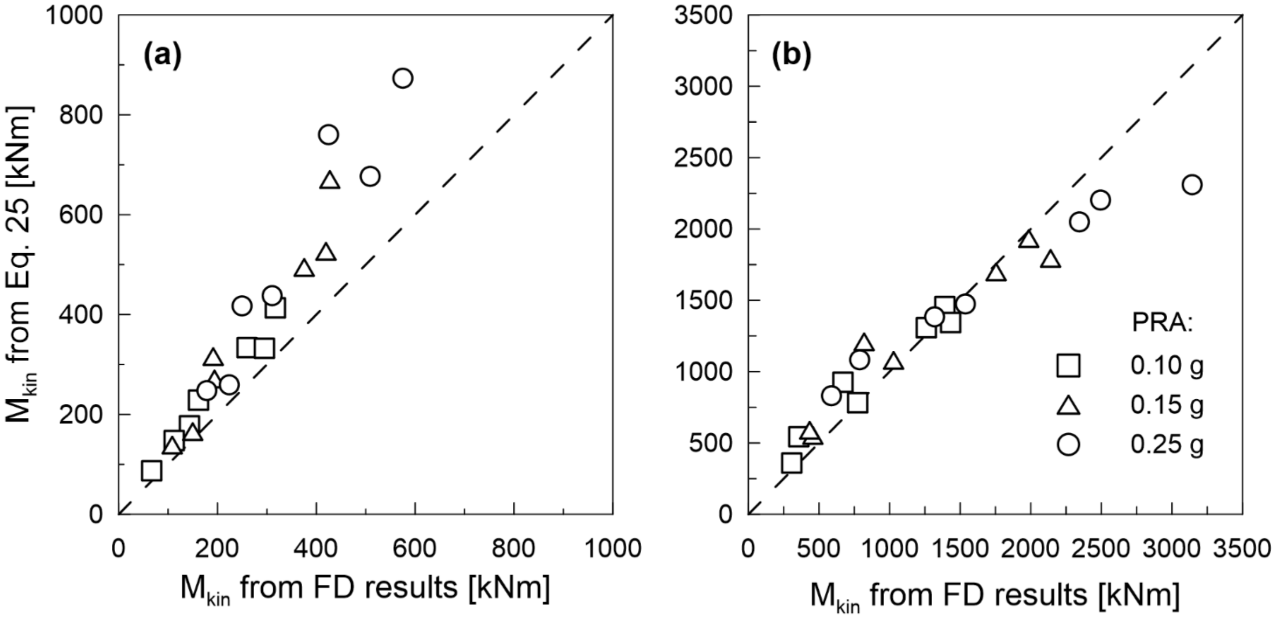

Figure 18: Comparison of kinematic pile-head bending moments between Equation 25 and FD results for (a) $d = 1$ m and (b) $d = 1.5$ m. Ground response parameters introduced in Equation 25 were obtained from DEEPSOIL NL analysis.

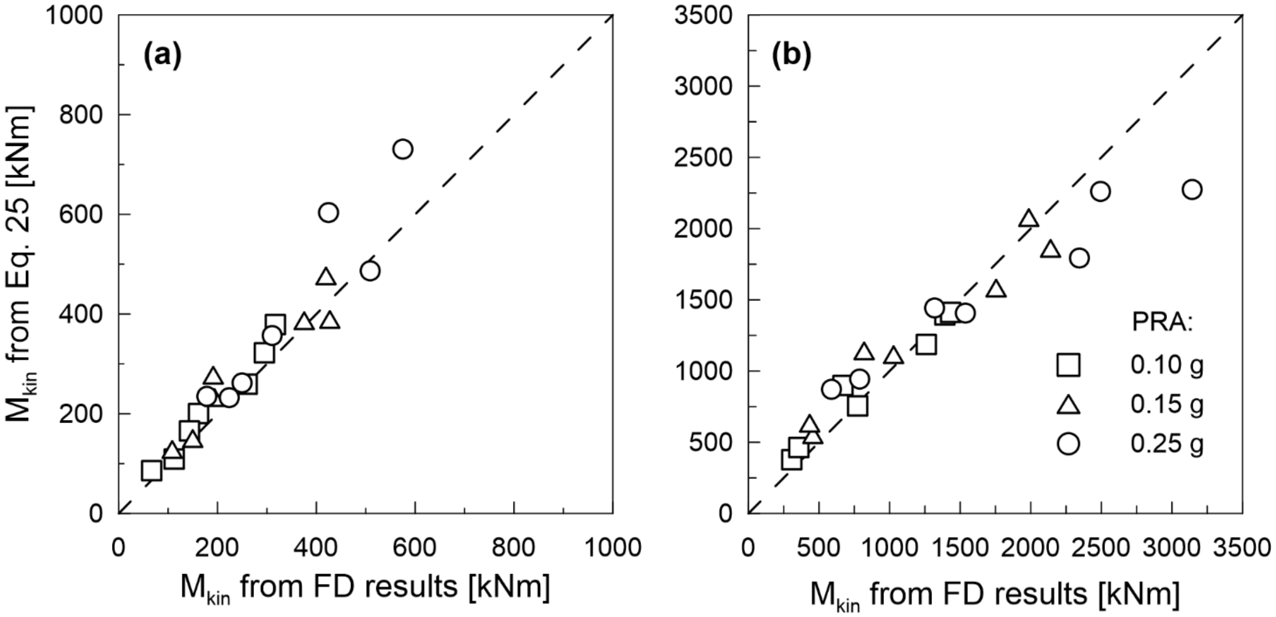

Figure 19: Comparison of kinematic pile-head bending moments between Equation 25 and FD results for (a) $d = 1$ m and (b) $d = 1.5$ m. Ground response parameters introduced in Equation 25 were obtained from FLAC analysis.

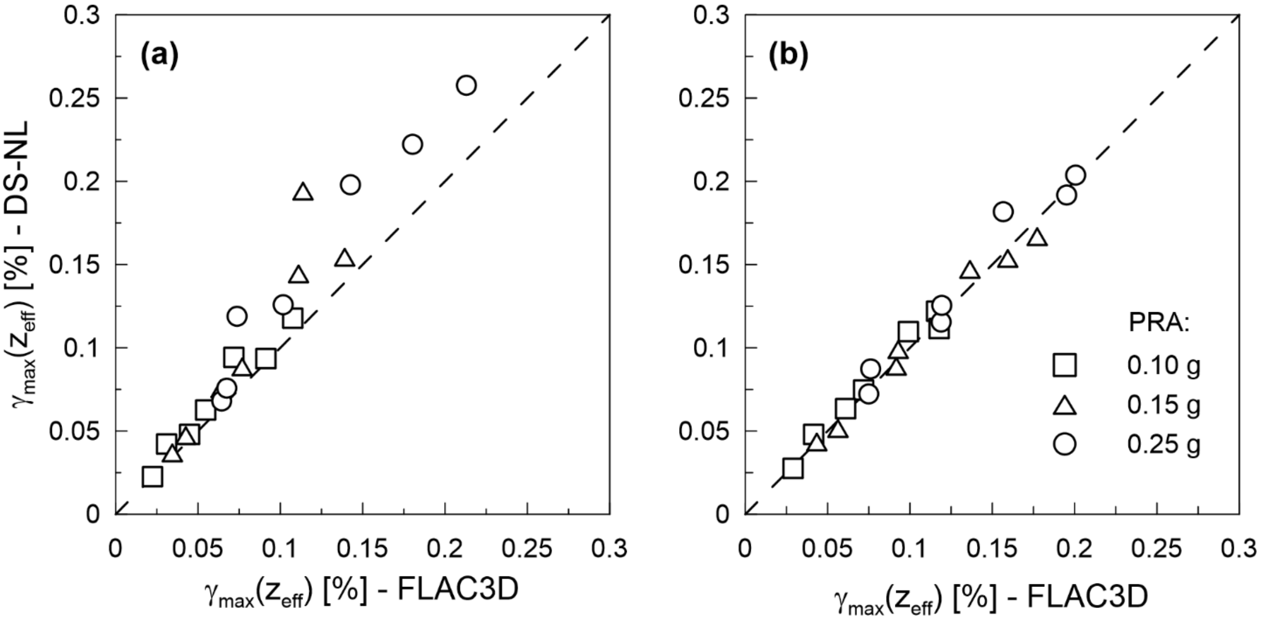

Figure 20: Comparison of maximum shear strain at z_{eff} between DEEPSOIL NL and FLAC analyses for (a) d = 1 m and (b) d = 1.5 m.

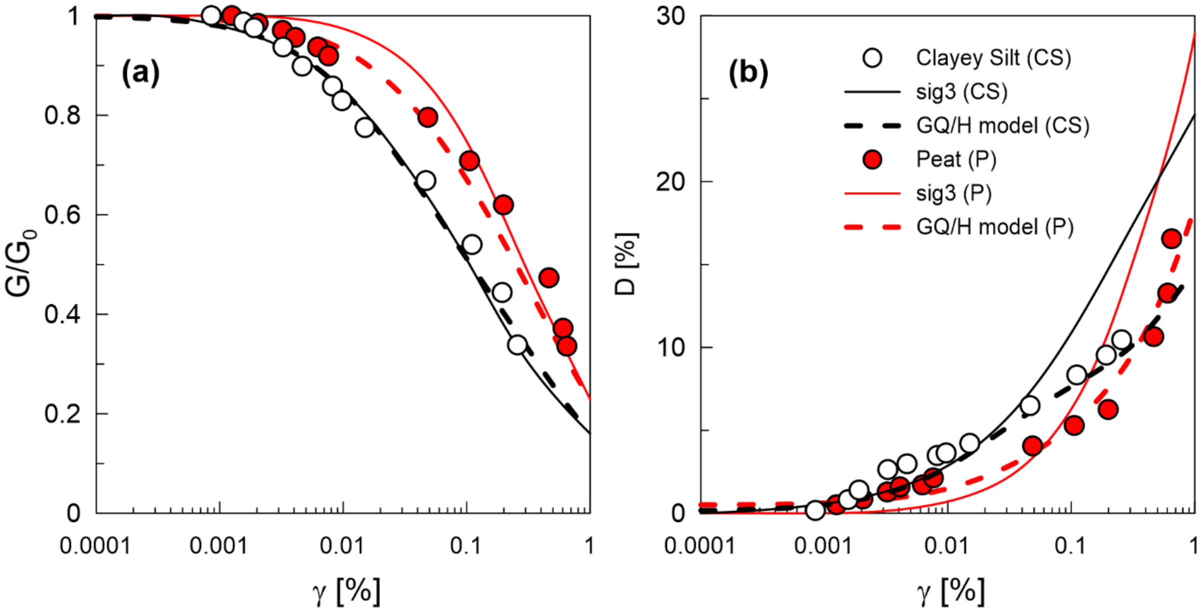

Figure 21: Comparison between experimental data (Clayey Silt and Peat layers) and GQ/H (constitutive model considered in DEEPSOIL analyses) and sig3 (constitutive model considered in FLAC3D analyses) soil models in terms of $G/G_0 - \gamma - D(\%)$ for the Po Valley case. (a) Stiffness degradation, (b) Hysteretic damping.

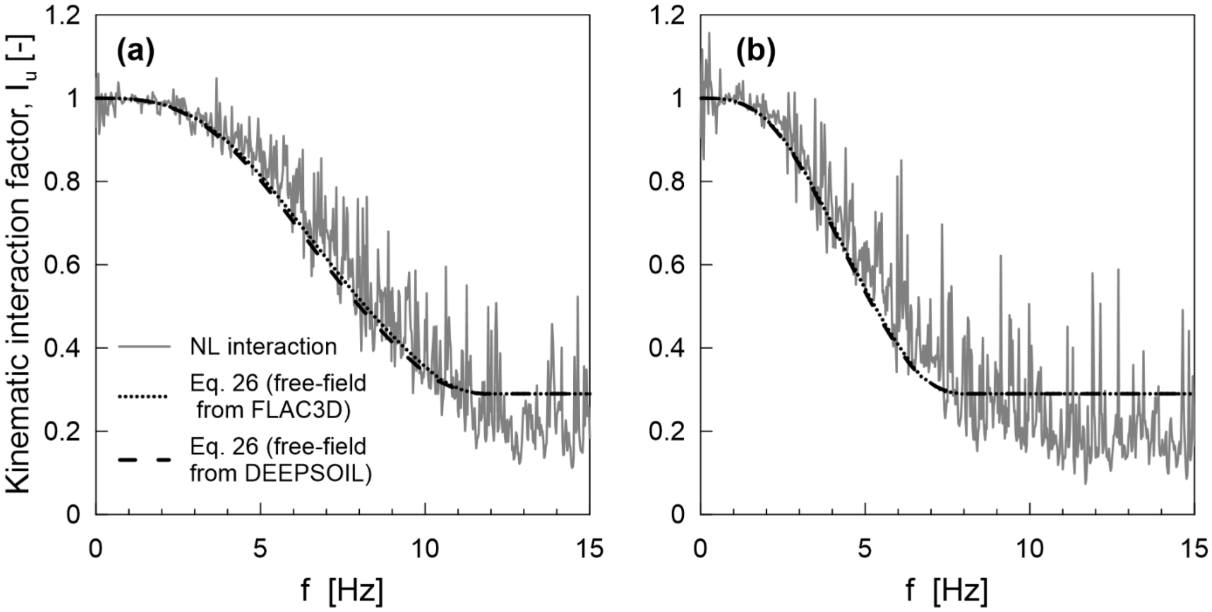

Figure 22: Amplitude of average kinematic interaction factor I_u derived by FLAC3D and Iovino et al. (2019) simplified formula for (a) d = 1 m and (b) d = 1.5 m. Plots refer to PRA = 0.15g.

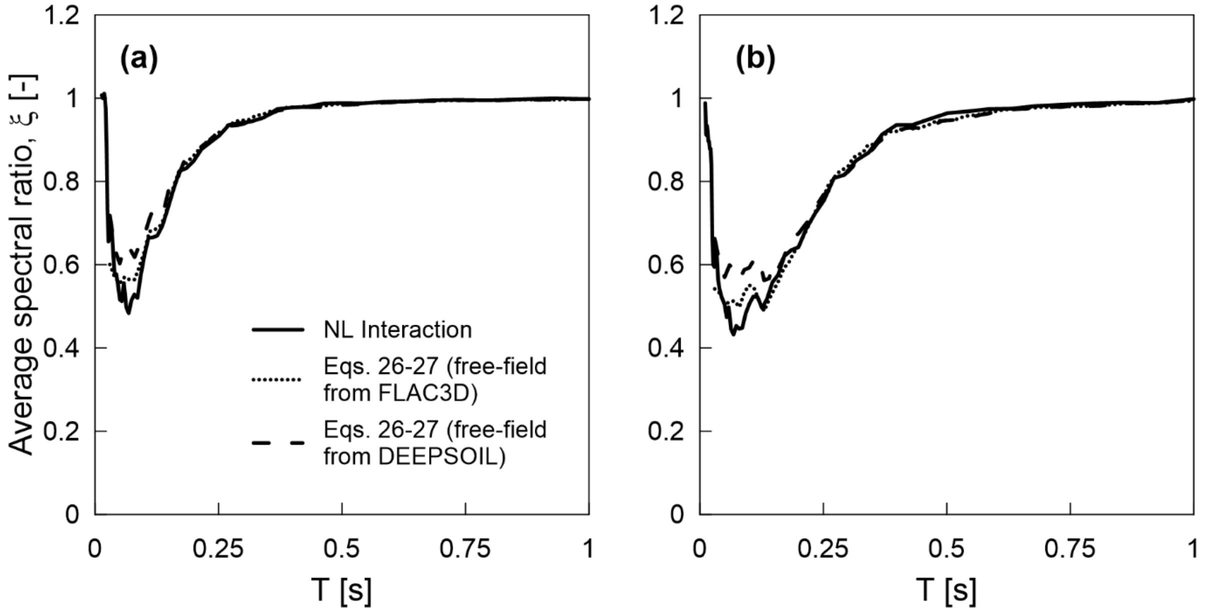

Figure 23: Comparison of average spectral ratios obtained with FLAC3D and Iovino et al. (2019) simplified procedure for (a) d = 1 m and (b) d = 1.5 m. Plots refer to PRA = 0.15g.

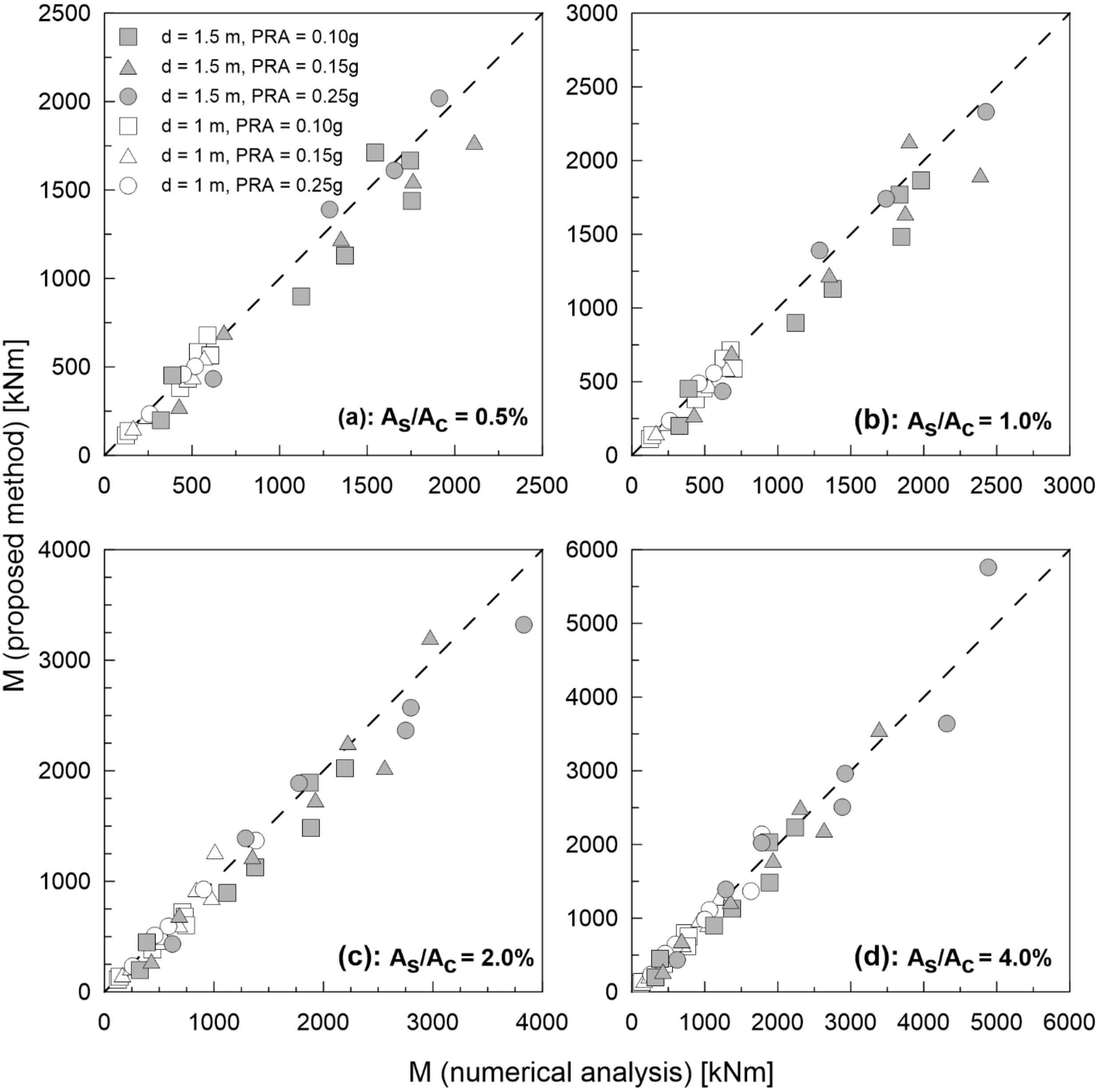

Figure 24: Comparison of kinematic pile-head bending moments between the proposed method and numerical results obtained with KIN-SP for different steel reinforcement ratios A_s/A_c at (a) 0.5%, (b) 1.0%, (c) 2.0% and (d) 4.0%.

Electronic supplement to

Kinematic soil-pile interaction under large earthquake-induced shear strains: An equivalent linear and static approach

by Stefano Stacul, Emmanouil Rovithis and Raffaele Di Laora

The results of a sensitivity analysis on critical modeling issues are presented in this supplement, towards the definition of the final 3D FLAC model employed in the paper. These issues refer to (i) modeling of the pile section, (ii) effect of model size and (iii) effect of model discretization. Comparative plots showing the effect of each modeling aspect on soil and pile response are discussed and the associated modeling choices are explained. Further details on the constitutive laws adopted with FLAC3D code to model soil behavior for each soil type under consideration are also reported.

Modeling of pile section

The concrete pile is modeled as a hybrid element (Fig. S1), composed of a beam element and surrounding solid elements, following the procedure described in Kimura and Zhang (2000). In this approach, the overall pile stiffness (axial stiffness, *EA* and flexural stiffness, *EI*) needs to be shared by the beam and the solid elements in a way that the pile cross-sectional flexural stiffness *EI* is equal to the sum of the beam element flexural stiffness $(EI)_{beam}$ and the flexural stiffness provided by the solid elements $(EI)_{solid}$. The same holds for the axial stiffness. The big advantage of the hybrid modelling of pile is that axial forces, bending moments and shear forces of the pile can be estimated easily from the software by exporting results for the beam element and then converting them for the hybrid system.

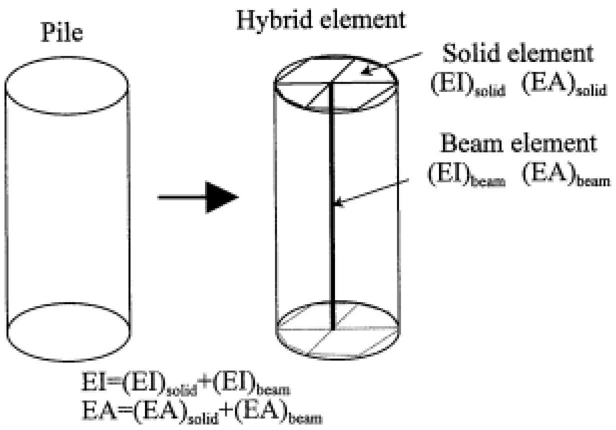

Fig. S1. Hybrid element: beam element and solid elements (Kimura and Zhang, 2000)

Following some preliminary analyses the sharing ratio of the flexural stiffness between the beam and the solid elements was set at 9 to 1, in agreement with relevant indications in Kimura and Zhang (2000).

The above selection took also into account that the solid elements should be stiff enough to represent the pile-size influence, thus the stiffness of the pile solid elements was considered large compared to the stiffness of the surrounding soil. This necessary stiffness contrast is satisfied by the assumption of an elastic modulus for the concrete pile at 25 GPa compared to the low-strain elastic modulus of the surrounding soil which falls in the range of 10-80 MPa for the soil cases under consideration.

The performance of the hybrid element against volume elements to model the pile section is shown in Figure 2 in terms of the generated bending moment envelope profile under the Coyote (Fig. S2a) and the Whittier Narrows (Fig. S2b) base motion, both scaled to PRA = 0.25g. These results refer to the pile embedded in the OC Clay. The differences between the two modeling approximations are negligible, which supports the choice of the hybrid element for modeling the pile.

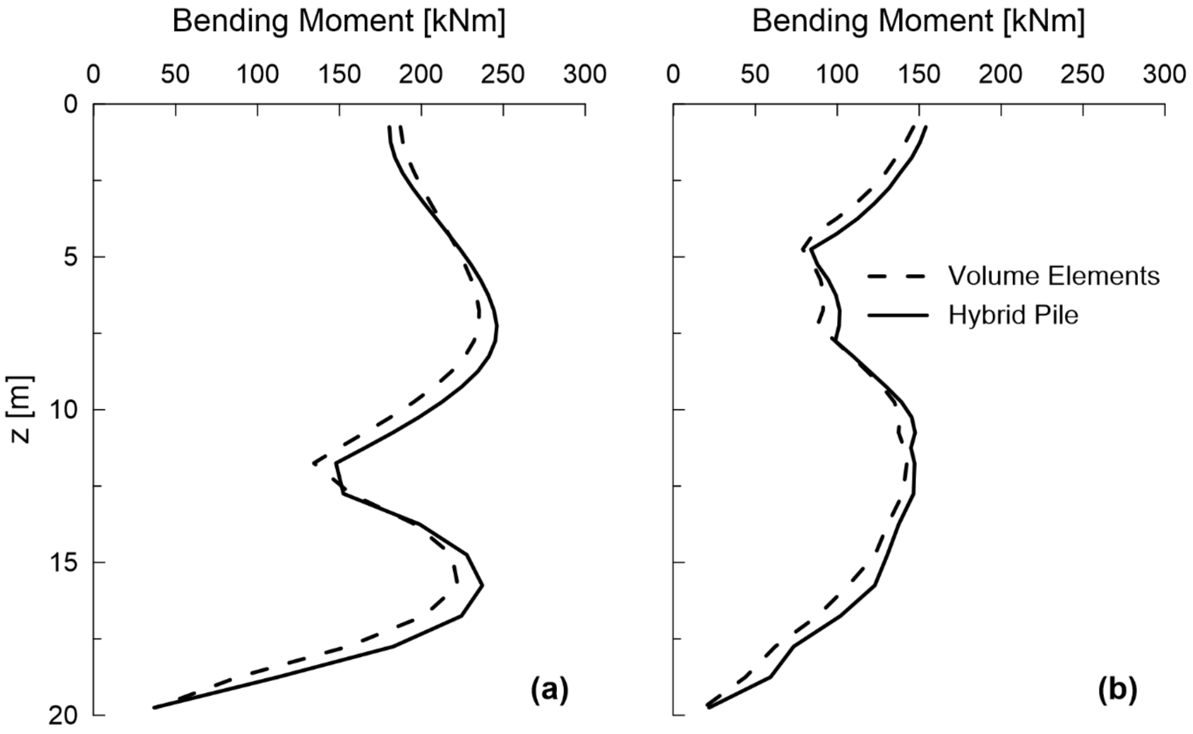

Fig. S2. Comparison of pile bending envelope (*M*) profiles between different modeling considerations for the pile section: CASE: OC clay, a_b=0.25g, input motions: Coyote (a), WhittierNarrows (b).

Effect of model size

The effect of model size was explored by analyzing four models with increasing plan dimensions referring to 10x10 m (Fig. S3a), 20x20 m (Fig. S3b), 30x30 m (Fig. S3c) and 40x40 m (Fig. S3d). The effect of the model size in terms of free-field maximum acceleration and shear strain profiles and pile bending moments envelope is shown in Fig. S4 and S5, for the OC Clay under the Coyote and the Whittier Narrows, representing a low- and a high-frequency motion, respectively, and peak rock acceleration PRA at 0.25g. A 30x30 m model was finally selected based on the negligible differences in response shown in Fig. S4 and S5.

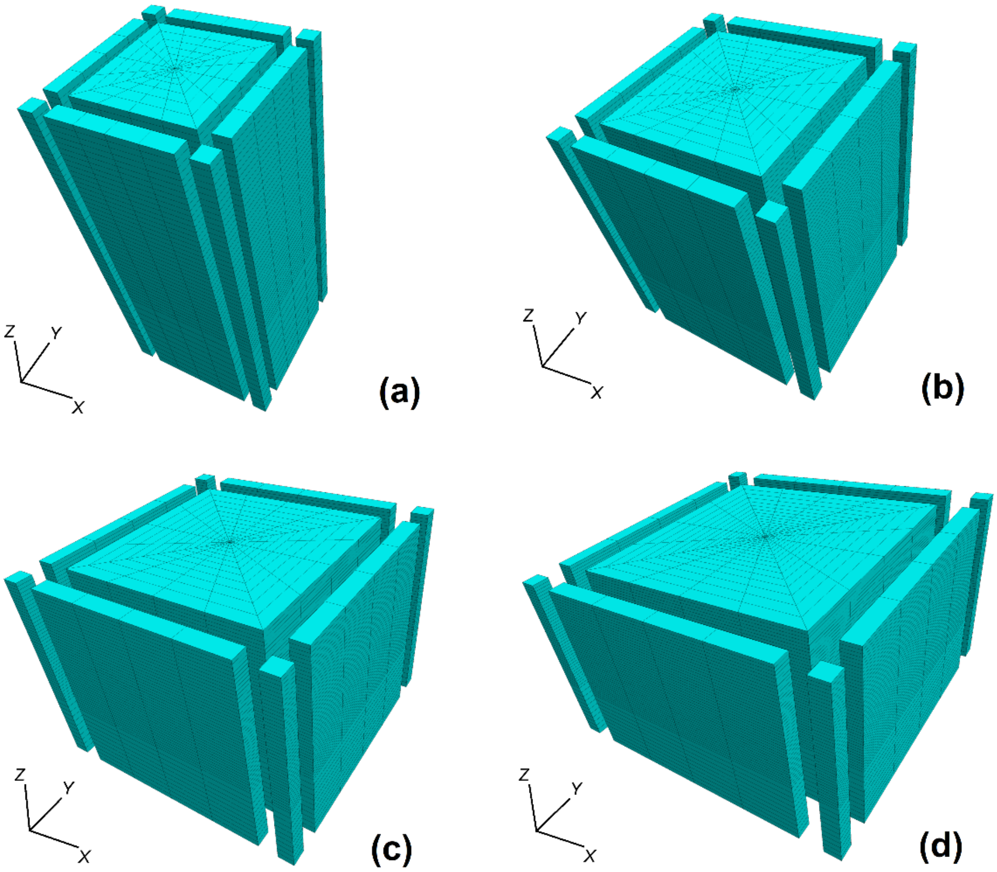

Fig. S3. Different models considered to explore the effect of model size by increasing plan dimensions: (a) 10x10 m (b) 20x20 m, (c) 30x30 m and (d) 40x40 m

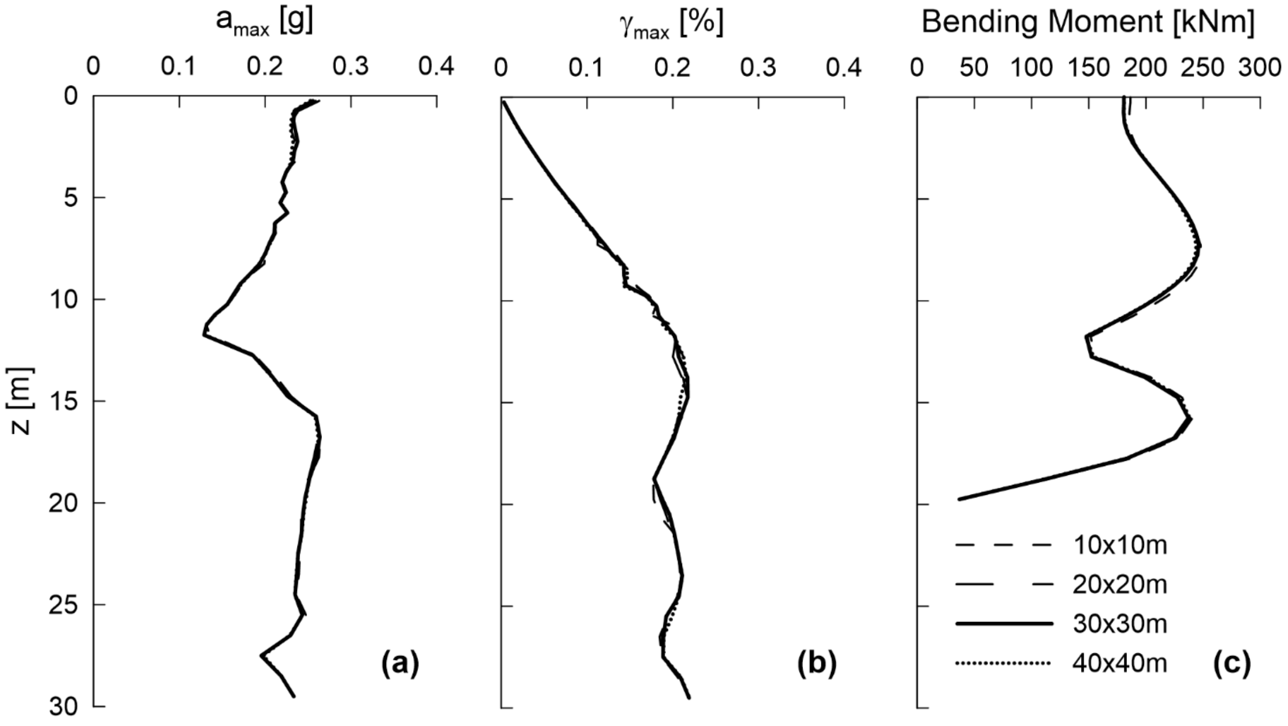

Fig. S4. Effect of model size on peak ground acceleration (a_{max}), max shear strain (γ_{max}) and pile bending envelope (M) profiles for the case of the OC Clay soil under the Coyote base excitation scaled to 0.25g.

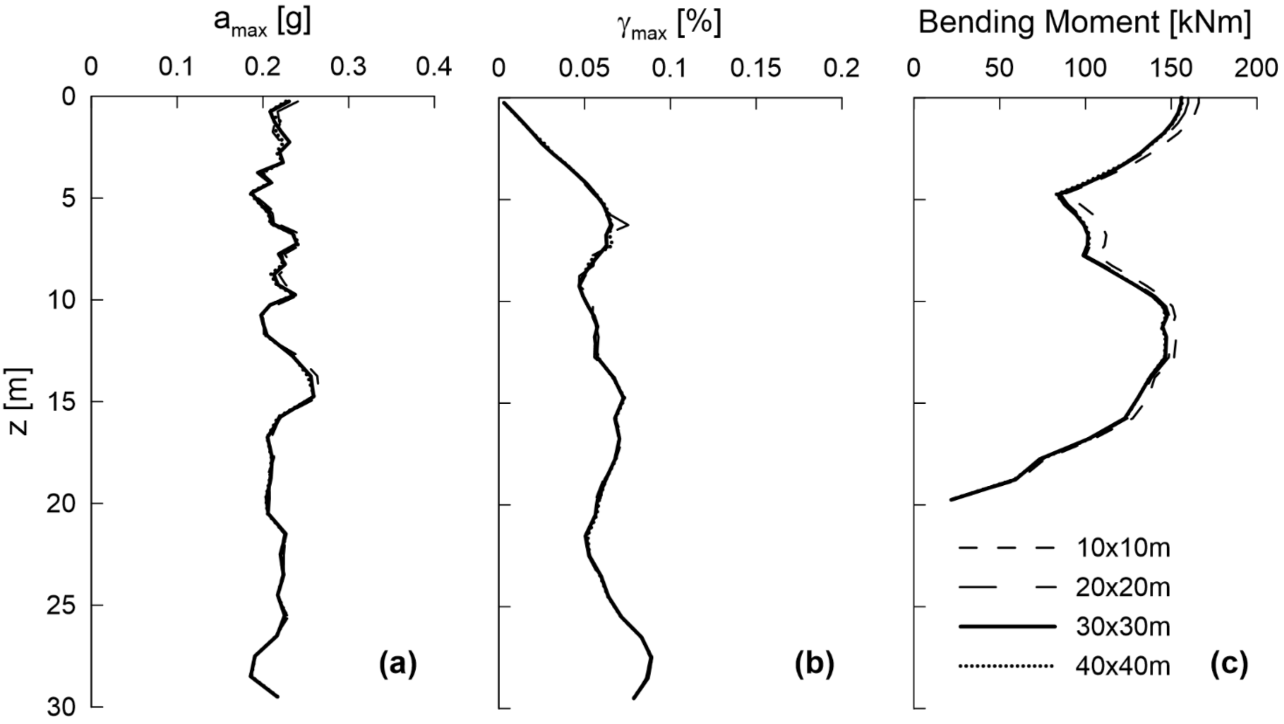

Fig. S5. Effect of model size on peak ground acceleration (a_{max}), max shear strain (γ_{max}) and pile bending envelope (*M*) profiles for the case of the OC Clay soil under the Whittier Narrows base excitation scaled to 0.25g.

Effect of model discretization

Having specified the model size at 30x30m in plan view, three discretization schemes were considered, as part of the parametric investigation in order to select the thickness (h_i) of the soil elements. The first scheme referred to h_i = 0.25 m for the first 20 m of the soil layer followed by h_i = 0.5 for the soil elements between 20 – 30 m. The second one was less dense considering h_i at 0.5 m and 1.0m between 0-20 m and 20-30 m, respectively. A constant value of h_i at 1.0 m along the whole soil layer was considered as a third discretization case.

The effect of the model discretization in terms of free-field maximum acceleration and shear strain profiles and pile bending moments envelope is shown in Fig. S6 and S7, for the NC Clay under the Coyote and the Whittier Narrows, respectively, scaled to peak rock acceleration PRA at 0.25g..

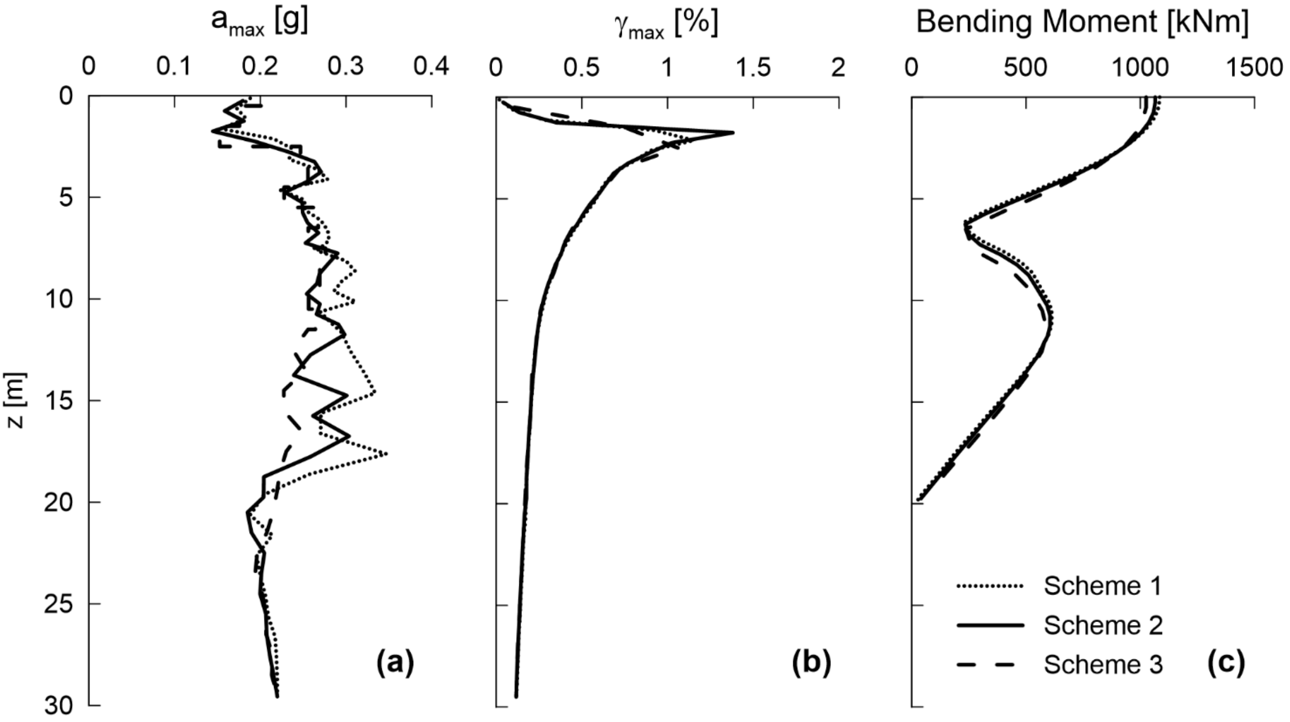

Fig. S6. Effect of model discretization on peak ground acceleration (a_{max}), max shear strain (γ_{max}) and pile bending envelope (M) profiles for the case of the NC Clay soil under the Coyote input motion scaled to 0.25g.

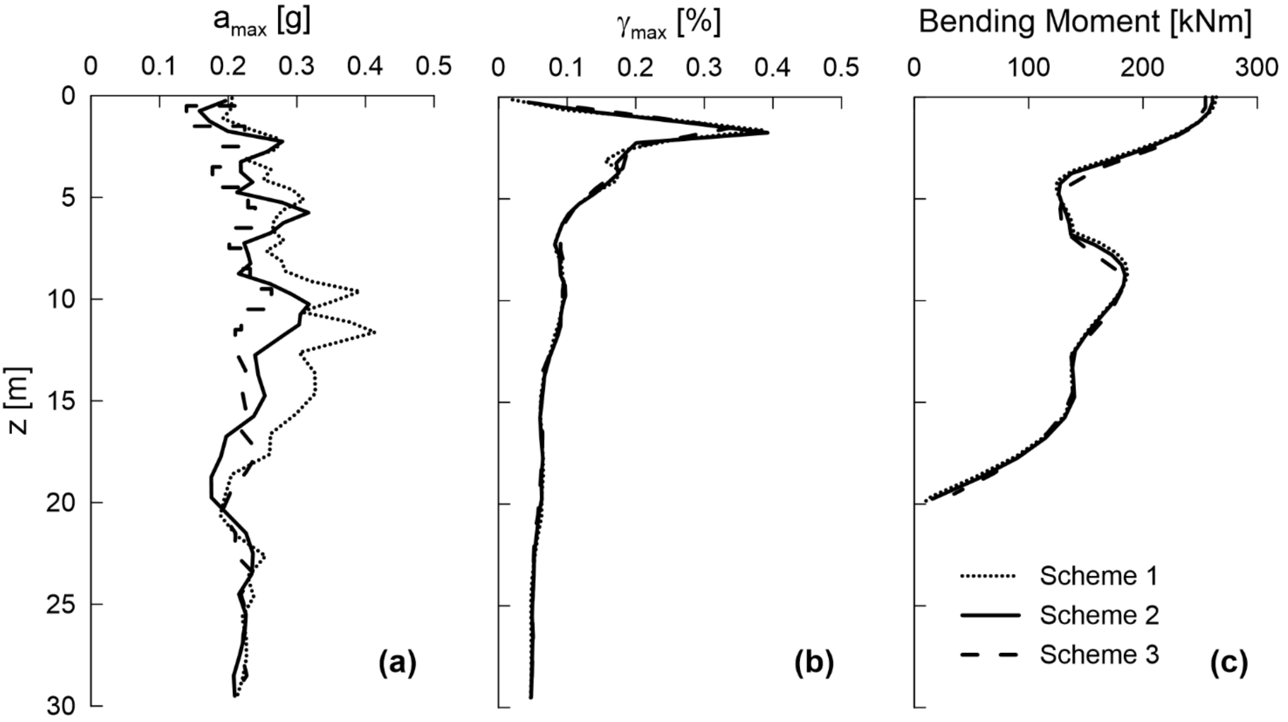

Fig.S7. Effect of model discretization on peak ground acceleration (a_{max}), max shear strain (γ_{max}) and pile bending envelope (M) profiles for the case of the NC Clay soil under the Whittier Narrows input motion scaled to 0.25g

Details on the constitutive laws employed in FLAC to model soil behavior

The hysteretic damping formulation available in FLAC3D should be used in conjunction with the built-in constitutive models. Thus, it is intended to provide damping for those models lacking intrinsic damping when not yielding.

If it is assumed that the shear stress depends only on the shear strain (not on the number of cycles, or time), one can derive an incremental constitutive relation from the degradation curve, described by $\tau/\gamma = G_s$, where τ is the shear stress, γ is the shear strain, and G_s is the secant shear modulus, as follows:

$$G_t = \frac{d\tau}{d\gamma} = G_s + \gamma \frac{dG_s}{d\gamma} \tag{S1}$$

which represents the "backbone curve" of the hysteretic model, where G_t is the tangent shear modulus.

Dry sand and OC Clay: FLAC "sig3" model

In the case of the dry sand, the Sigmoidal model "sig3" available in FLAC was adopted, in conjunction with a linear elastic constitutive model, to introduce hysteretic damping. The above "sig3" model function is:

$$\frac{G_s}{G_0} = \frac{a}{1+\exp(-(\log_{10}\gamma - x_0)/b)} \tag{S2}$$

For the dry sand profile, the parameters a, b and x_0 introduced in the above expression were set at 1.014, -0.4792 and -1.249, respectively. The outcome of the "sig3" model fit to the reference "sand-upper range" G_s/G_0 - γ - $D(\%)$ curves defined in Seed and Idriss (1970) is shown in Fig. S8a and S8b. The corresponding fit in terms of the backbone curve (τ - γ) is plotted in Fig. S8c. For the OC clay soil, the "sig3" model parameters were set equal to: a = 1.017, b = -0.587 and x_0 = -0.633. For these values, the model fit to the reference Vucetic and Dobry (1991) curves for I_P = 40% is shown in Fig. S9.

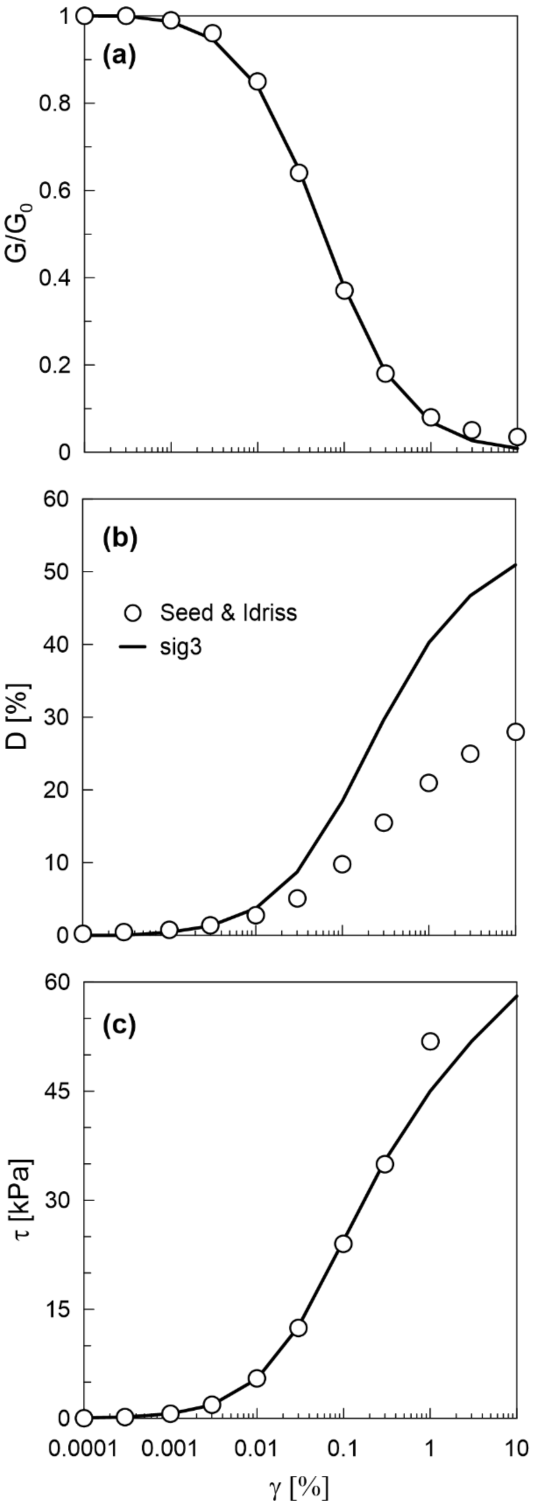

Fig. S8. G_s/G_0-γ; D-γ and τ-γ curves for the dry sand material (V_s = 200 m/s).

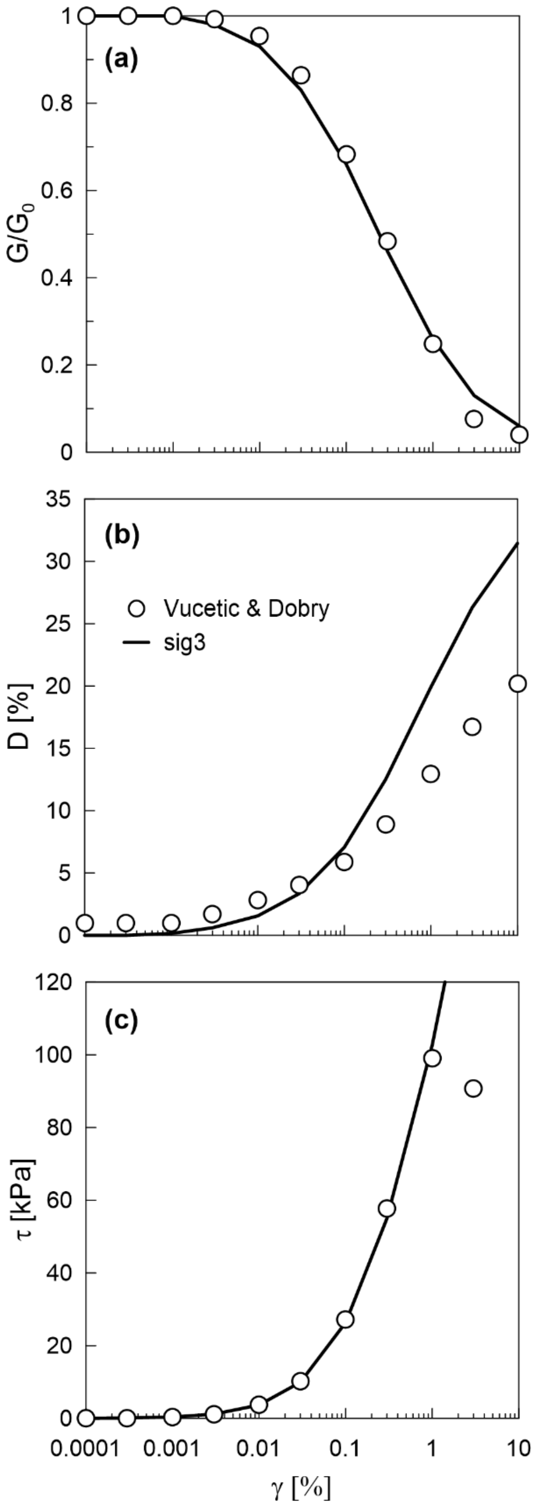

Fig. S9. G_s/G_0-γ; D-γ and τ-γ curves for the OC clay material (V_s = 140 m/s).

NC Clay: USCDClay model

For the particularly soft NC Clay under consideration, the sig3 hysteretic model was considered inappropriate since it does not consider the shear strength of the soil as part of the model parameters. To this end, a 3D elasto-plastic material model which reproduces nonlinear hysteric shear behavior and accumulation of permanent shear deformation was introduced to FLAC3D. The above constitutive law refers to the UCSDClay model developed by Elgamal et al. 2008. The input parameters for the UCSDClay model are: the saturated soil mass density (ρ_{sat} in ton/m^3), the low-strain shear modulus (G_0), the Poisson's ratio (ν), the shear strength (s_u), the shear strain at which the shear strength is reached (γ_{peak}) and the number of yield surfaces (N_{ys}). For the NC clay under consideration, the G_0 and s_u values inputted in the UCSDClay model are those specified in Fig. 1 of the paper, while ρ_{sat}, ν, γ_{peak} and N_{ys} were set equal to 1.8 ton/m^3, 0.4, 10% and 30, respectively, following the recommendations reported in SoilQuake website (http://www.soilquake.net/ucsdsoilmodels/parameters.html). The USCDClay model calibration to the reference G_s/G_0 - γ - $D(\%)$ curves by Vucetic and Dobry (1991) for I_P = 40% is shown in Fig. 4 of the paper.

Effect of soil-pile interface elements

FLAC3D allows the definition of interface elements that are characterized by Coulomb sliding and/or tensile and shear bonding. In the herein reported sensitivity analyses, the parameters of friction, cohesion, normal stiffness and shear stiffness were considered. Friction and cohesion were set according to the surrounding soil strength parameters. The values of normal (k_n) and shear stiffnesses (k_s) were assessed following the FLAC3D manual suggestions. The good rule-of-thumb (suggested in FLAC3D documentation) is that k_n and k_s be set to ten times the equivalent stiffness of the stiffest neighboring zone. The apparent stiffness (expressed in stress-per-distance units) of a zone in the normal direction is given by $\max\{[K+(4/3)G/\Delta z_{\min}]\}$, where: K and G are the bulk and shear modulus, respectively; and Δz_{min} is the smallest width of an adjoining zone in the normal direction. The *max[ ]* notation indicates that the maximum value over all zones adjacent to the interface is to be used (there may be several materials adjoining the interface). In the analyses involving interface elements, a small amount (0.1-0.2 %) of viscous Rayleigh damping was added. Representative comparisons between different modeling assumptions for the soil-pile interface (i.e. with and without interface elements) are shown in the Figs. S10, S11 and S12, referring to different combinations of soil profile and base excitations. The negligible differences allow the assumption of a bonded connection between soil and pile elements adopted in the final FLAC3D model reported in the paper.

Further support on the minor effect of interface elements on pile's kinematic response is provided by the low contact stresses between soil and pile developed under kinematic loading compared to those generated under an inertial force imposed at the pile head. In order to highlight better this aspect, Fig.S13 shows a comparison between kinematic and inertial soil-pile interaction in terms of soil reaction (p) and pile/soil displacement profiles. The kinematic analysis results refer to the idealized OC clay profile under the WhittierNarrows input motion scaled to PRA = 0.15g, while the inertial analysis was performed for a static lateral load of 100 kN applied at the head of the pile, which produces the same pile-head bending moment as the kinematic one. For the inertial case, results were obtained with the p-y curve based code RSPile considering the p - y curves for submerged stiff clay (Reese, et al., 1975). It is observed that pile-soil relative displacements and therefore soil reactions (p) are extremely larger in the inertial case close to the pile-head and diminish faster with depth until the pile's active length. This means that for the inertial case, modeling of the soil-pile interface is of major concern since a relative slip between soil and pile may occur. On the contrary, under kinematic loading as the relative pile-soil displacement is quite lower, interface modeling will have a minor effect on the overall response.

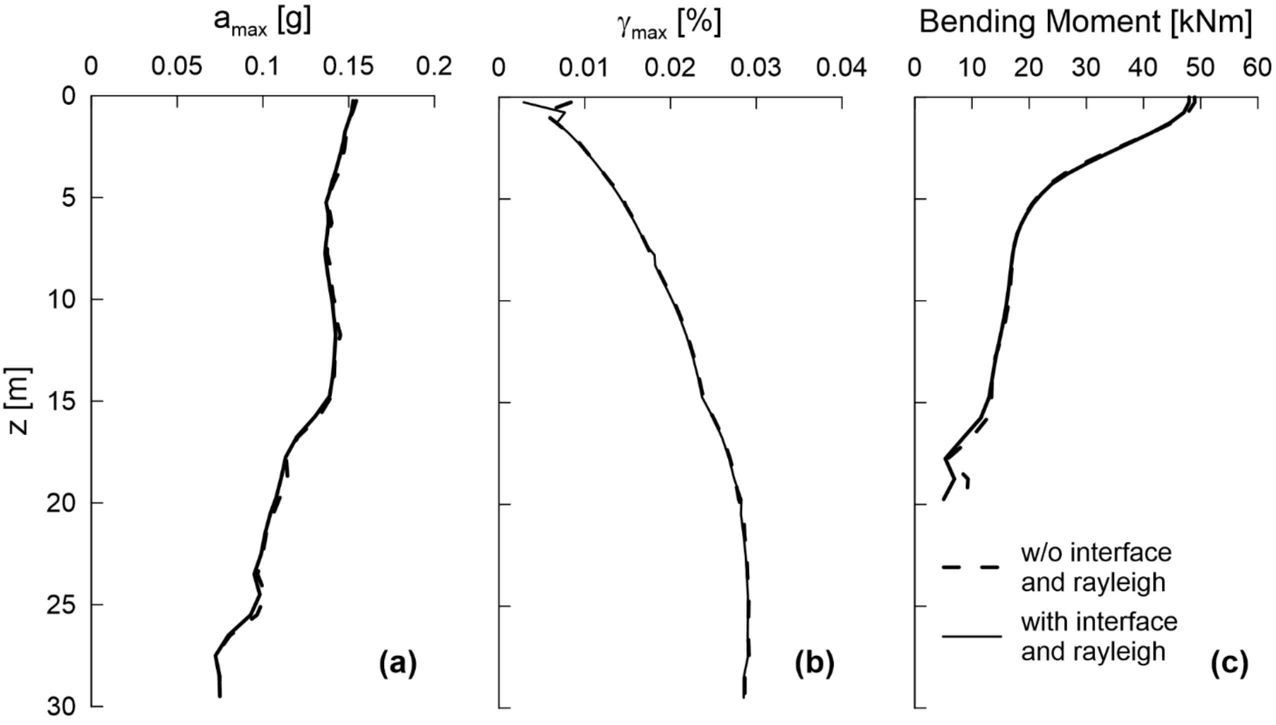

Fig. S10. Peak acceleration (a_{max}), max shear strain (γ_{max}) and pile bending envelope (M) profiles for the case of sand under the Coyote input motion scaled to 0.10g.

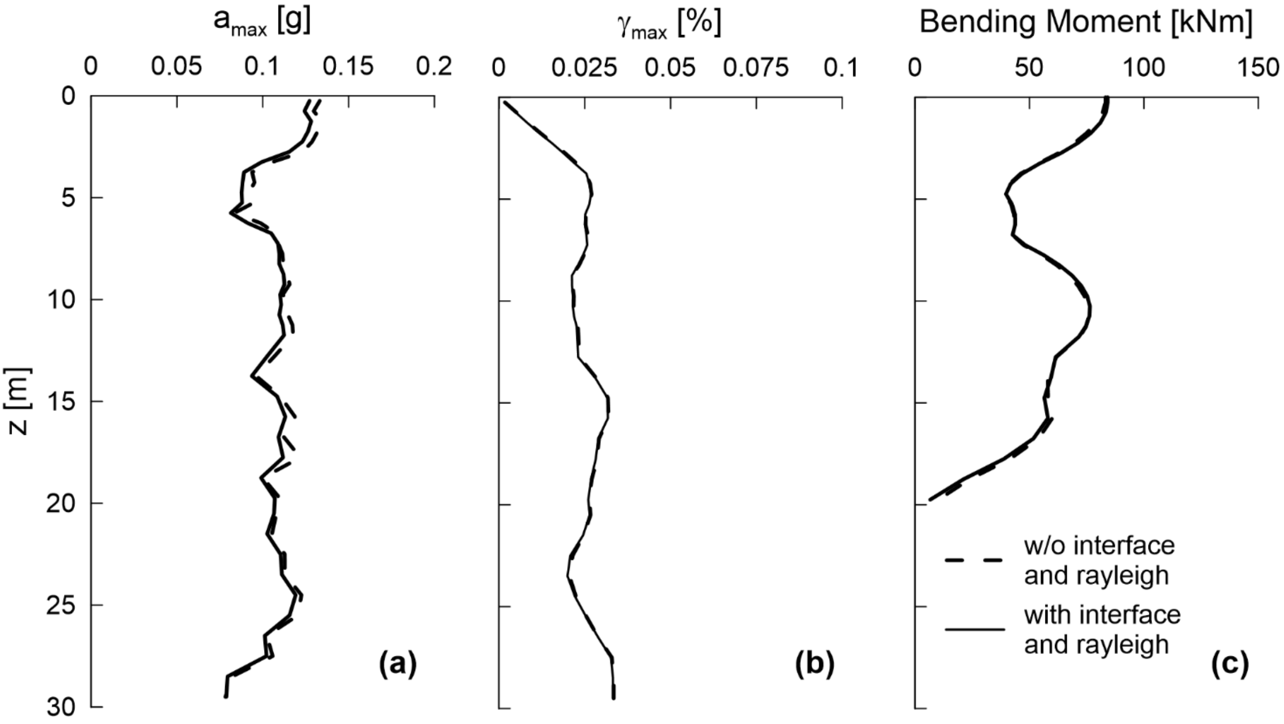

Fig. S11. Peak acceleration (a_{max}), max shear strain (γ_{max}) and pile bending envelope (M) profiles for the case of OC Clay under the Whittier Narrows input motion scaled to 0.10g.

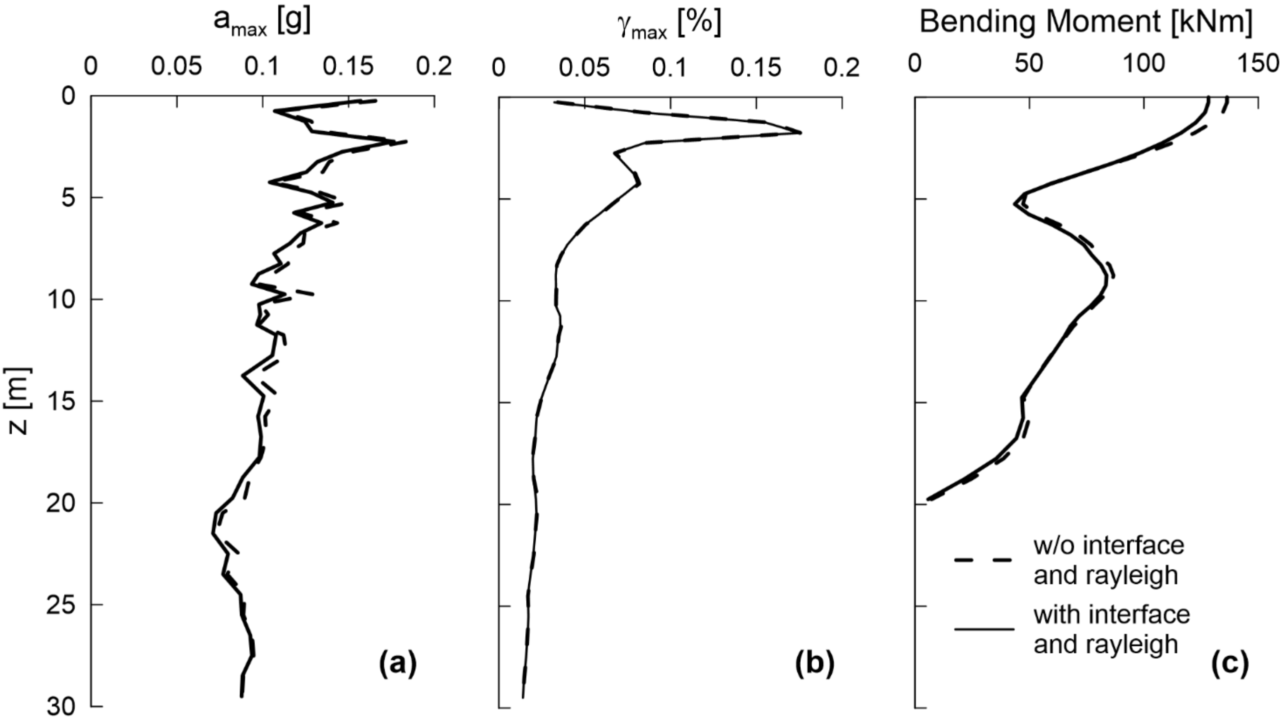

Fig. S12. Peak acceleration (a_{max}), max shear strain (γ_{max}) and pile bending envelope (M) profiles for the case of NC Clay under the Whittier Narrows input motion scaled to 0.10g.

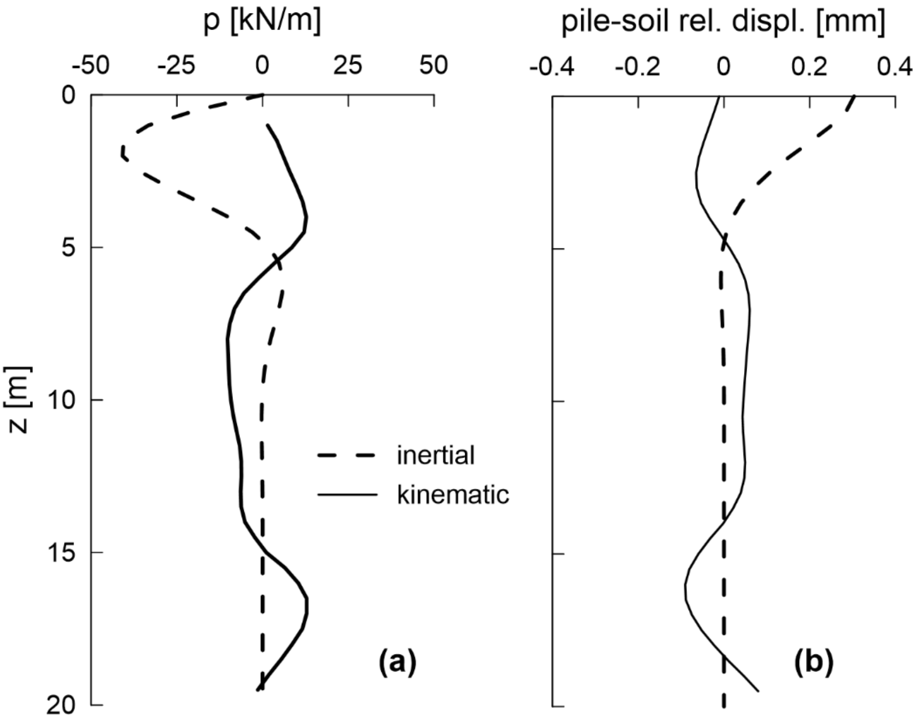

Fig. S13. Comparison between kinematic and inertial soil-pile interaction in terms of (a) soil reaction and (b) pile-soil relative displacement profiles.

Free-field ground response for PRA = 0.10g and 0.15g (NC Clay profile)

In Figs. S14 and S15 soil response analysis results inferred via DEEPSOIL (EL and NL) and FLAC3D for the idealized NC clay soil profile are shown.

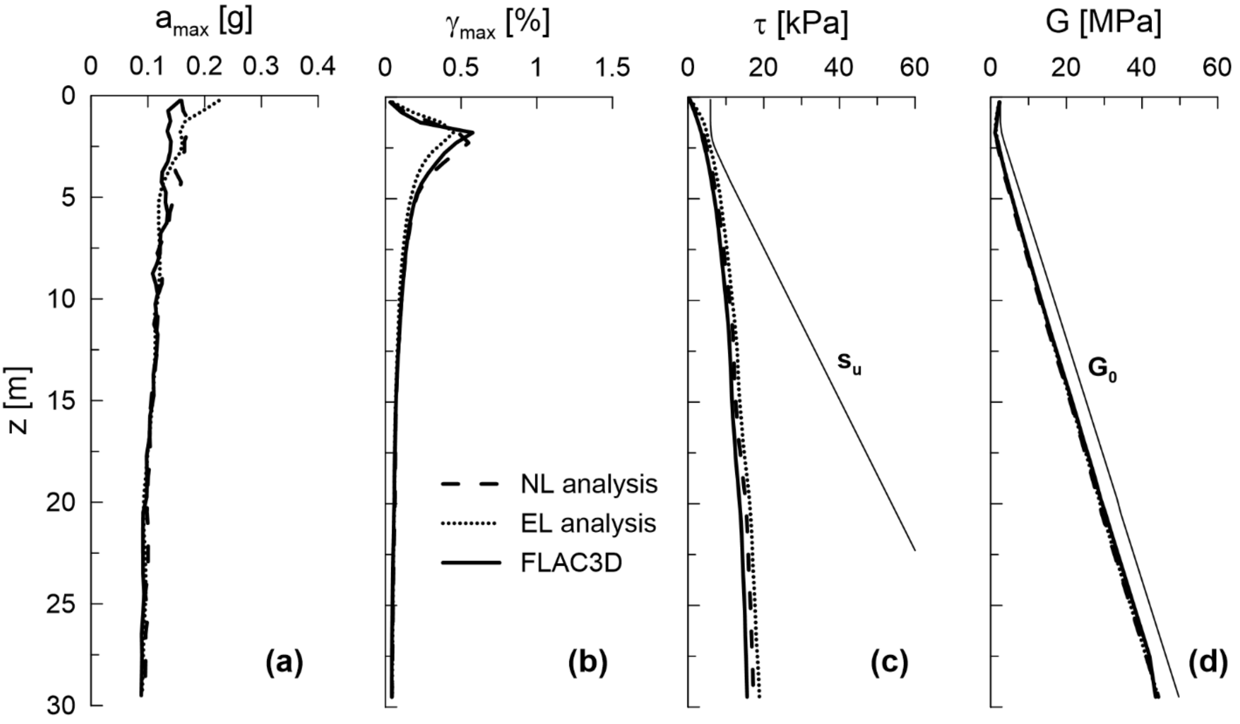

Fig. S14: Comparison of free-field ground response analysis results between DEEPSOIL (EL and NL analysis) and FLAC3D for the NC clay profile in terms of: (a) average PGA profile (b) average maximum shear strain profile (c) average shear stress and (d) mobilized shear modulus *G* with depth. All plots refer to PRA = 0.10g.

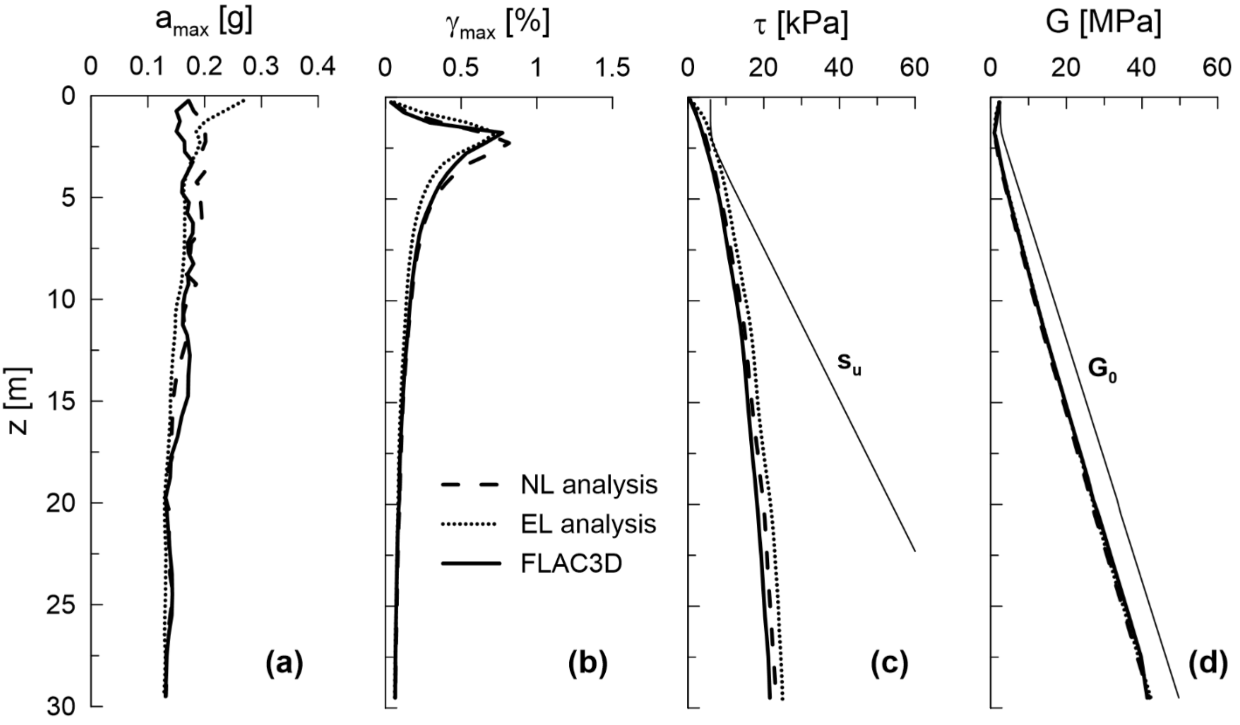

Fig. S15: Comparison of free-field ground response analysis results between DEEPSOIL (EL and NL analysis) and FLAC3D for the NC clay profile in terms of: (a) average PGA profile (b) average maximum shear strain profile (c) average shear stress and (d) mobilized shear modulus *G* with depth. All plots refer to PRA = 0.15g.

References

Elgamal, A., Yan, L., Yang Z., and Conte., J. P. 2008. Three-dimensional seismic response of Humboldt Bay bridge foundation-ground System, Journal of Structural Engineering, ASCE, 134(7): 1165-1176.

Kimura, M., & Zhang, F. 2000. Seismic evaluations of pile foundations with three different methods based on three-dimensional elasto-plastic finite element analysis. Soils and Foundations, 40(5): 113-132.

Masing, G. 1926. Eigenspannumyen und verfeshungung beim messing. In Proc. Inter. Congress for Applied Mechanics (pp. 332-335).

Reese, L., W. Cox, and F. Koop 1975. Field testing and analysis of laterally loaded piles in stiff clays. In Proc. 7th Offshore Technology Conference, Volume 2, OTC 2312, pp. 671–690. Houston, TX.

Seed, H. B. and Idriss, I. M. 1970. Soil Moduli and Damping Factors for Dynamic Response Analyses. Report EERC 70-10, Earthquake Engineering Research Center, University of California, Berkeley.

Vucetic, M. and Dobry, R. 1991. Effect of soil plasticity on cyclic response. Journal of Geotechnical Engineering, 17: 89-107.